Check for updates

BREAKTHROUGH REPORT

CRISPR-TSKO: A Technique for Efficient Mutagenesis in Specific Cell Types, Tissues, or Organs in Arabidopsis[OPEN]

Ward Decaestecker,[a,b,1] Rafael Andrade Buono,[a,b,1] Marie L. Pfeiffer,[a,b] Nick Vangheluwe,[a,b] Joris Jourquin,[a,b] Mansour Karimi,[a,b] Gert Van Isterdael,[c,d] Tom Beeckman,[a,b] Moritz K. Nowack,[a,b,2] and Thomas B. Jacobs[a,b,2]

[a] Department of Plant Biotechnology and Bioinformatics, Ghent University, Technologiepark 71, 9052 Ghent, Belgium
[b] VIB Center for Plant Systems Biology, Technologiepark 71, 9052 Ghent, Belgium
[c] VIB Flow Core, VIB Center for Inflammation Research, Technologiepark 71, B-9052 Ghent, Belgium
[d] Department of Biomedical Molecular Biology, Ghent University, Ghent, Belgium

ORCID IDs: 0000-0003-0247-3189 (W.D.); 0000-0002-6675-3836 (R.A.B.); 0000-0002-5360-054X (M.L.P.); 0000-0002-4885-6161 (N.V.); 0000-0003-0808-0730 (J.J.); 0000-0002-0246-9318 (M.K.); 0000-0001-6626-1316 (G.V.I.); 0000-0001-8656-2060 (T.B.); 0000-0001-8918-7577 (M.K.N.); 0000-0002-5408-492X (T.B.J.)

Detailed functional analyses of many fundamentally important plant genes via conventional loss-of-function approaches are impeded by the severe pleiotropic phenotypes resulting from these losses. In particular, mutations in genes that are required for basic cellular functions and/or reproduction often interfere with the generation of homozygous mutant plants, precluding further functional studies. To overcome this limitation, we devised a clustered regularly interspaced short palindromic repeats (CRISPR)-based tissue-specific knockout system, CRISPR-TSKO, enabling the generation of somatic mutations in particular plant cell types, tissues, and organs. In Arabidopsis (*Arabidopsis thaliana*), CRISPR-TSKO mutations in essential genes caused well-defined, localized phenotypes in the root cap, stomatal lineage, or entire lateral roots. The modular cloning system developed in this study allows for the efficient selection, identification, and functional analysis of mutant lines directly in the first transgenic generation. The efficacy of CRISPR-TSKO opens avenues for discovering and analyzing gene functions in the spatial and temporal contexts of plant life while avoiding the pleiotropic effects of system-wide losses of gene function.

INTRODUCTION

The generation of stable, inheritable loss-of-function mutant alleles has been indispensable for functional genomic studies in plants. Such knockout or knockdown lines have been generated using various techniques such as ionizing radiation, ethyl methanesulfonate, T-DNA or transposon insertions, RNA interference (RNAi), or artificial microRNAs. In recent years, there has been an explosion in the generation of knockout plant lines via clustered regularly interspaced short palindromic repeats (CRISPR) technology.

CRISPR technology contains two components, the CRISPR-associated (Cas) nuclease and CRISPR RNAs that direct the nuclease to the target nucleic acid. The most commonly used CRISPR system in plants is based on the Cas9 DNA endonuclease and its artificial CRISPR RNA, the guide RNA (gRNA; Jinek et al., 2012). In plants, Cas9 is very efficient at inducing double-strand

DNA breaks. DNA breaks repaired by the error-prone non-homologous end-joining pathway ultimately result in the formation of short insertions and/or deletions (indels) at the break site (Bortesi and Fischer, 2015). These indels most often lead to frame shifts and/or early stop codons, effectively generating knockout mutations in the targeted gene(s).

Most CRISPR efforts in plants to date have focused on generating stable and heritable mutant alleles for reverse genetics approaches. Yet this approach is limited, as the knockout of many fundamentally important genes convey severe pleiotropic phenotypes or even lethality. Of the ~25,000 protein-coding genes in the Arabidopsis (*Arabidopsis thaliana*) genome, 10% are estimated to be indispensable (Lloyd et al., 2015). This presents a considerable challenge for functional analyses of genes with essential functions.

An approach to overcome these problems is the use of tissue-specific gene silencing (Alvarez et al., 2006; Schwab et al., 2006). However, gene silencing is often incomplete, interfering with the interpretation of the observed phenotypes. Furthermore, it has been well established that small RNAs can be mobile (Melnyk et al., 2011), limiting the tissue specificity in gene-silencing experiments. Therefore, the results obtained using gene silencing are often not comparable with those obtained using stably transmitted DNA-based mutants. Transgenic vectors generating dominant-negative protein versions have been developed for certain genes. Expressing these mutant versions in

IN A NUTSHELL

Background: As plant molecular geneticists, we work to understand how gene functions shape plant growth and development. Our standard approach to study gene function has been to first eliminate (or knockout) a gene by mutating the plant's DNA. These mutations are permanent and can be passed on to the offspring. This allows us to perform experiments comparing plants with and without this individual gene. However, it is thought that ~10% of plant genes are so fundamentally important that it is impossible to make such a mutant without killing or severely affecting the entire plant. This prevents us from studying the functions of some really important genes. For example, *PDS3* is an essential gene for chloroplast formation, and conventional mutants are completely white and cannot survive for very long.

Question: We wanted to develop a technology to overcome this restriction. For that we turned to CRISPR technology, as it can very effectively generate DNA mutations. We wanted to see if it was possible to make DNA mutations only in specific cells by having CRISPR activated only in those cell types.

Findings: We developed a CRISPR system we call CRISPR-TSKO for **t**issue-**s**pecific **k**nock**o**ut. We demonstrate the use of CRISPR-TSKO by mutating several essential genes in either different parts of the root or stomata (small openings on the leaves facilitating air exchange). The mutated plants all grew normally, but upon closer inspection of the roots or stomatal cells, we could see the effects of the mutations we made. For example, when we targeted *PDS3* specifically in the stomata, plants developed normally but lacked chloroplasts in the stomatal cells. These plants can now be used to investigate the specific role of chloroplasts in stomatal function. In addition, we made a user-friendly toolkit that allows us to easily modify CRISPR-TSKO so it is active in different cells or to easily target different genes.

Next steps: The versatility of CRISPR-TSKO will enable us and other researchers to mutate and investigate the functions of fundamentally important genes in specific cells, tissues, or organs during various processes of plant growth and development.

a tissue-specific context can locally interfere with endogenous gene functions (Fukaki et al., 2005; Mitsuda et al., 2011). Other methods include the conditional knockout of genes in specific cell types or tissues using a CRE recombinase (Sieburth et al., 1998). These approaches, however, can be cumbersome and difficult to scale (Muñoz-Nortes et al., 2017).

Outside of the plant field, researchers have recently overcome such limitations with the development of conditional knockouts using CRISPR technology. In zebrafish (*Danio rerio*), the *gata1* promoter driving Cas9 expression was used to knock out genes specifically in the erythrocytic lineage (Ablain et al., 2015). In *Drosophila melanogaster*, targeted knockout mutations in two essential genes, *Wingless* and *Wntless*, only in germ cells permitted the generation of adult flies, whereas ubiquitous knockout individuals did not survive past the pupal stage (Port et al., 2014). Additionally, cardiomyocyte-specific expression of Cas9 led to organ-specific knockout in a mouse model (Carroll et al., 2016). The use of tissue-specific promoters to drive Cas9 expression has been reported in plants (Hyun et al., 2015; Yan et al., 2015; Mao et al., 2016). However, these efforts have focused on increasing the recovery of stably transmitted mutant alleles. Recently, the fiber-specific *NST3/SND1* promoter was used to drive Cas9 expression and target the essential gene *HCL* (encoding a hydroxy-cinnamoyl transferase) in Arabidopsis (Liang et al., 2019). This approach demonstrated that xylem-specific Cas9 expression is able to specifically decrease lignin content in xylem cells while avoiding the strong pleiotropic growth defects of full knockout mutants.

Here, we present a method for tissue-specific genome modification via a CRISPR tissue-specific knockout (CRISPR-TSKO) vector system in Arabidopsis that allows for the specific generation of somatic DNA mutations in plants. The CRISPR-TSKO toolset is simple to use, highly efficient, and allows for multiplexing and large-scale screening approaches. We demonstrate the potential of CRISPR-TSKO for somatic gene knockouts of several essential genes in diverse plant cell types, tissues, and organs. We also detail important considerations and limitations for the use of CRISPR-TSKO and provide best practices for researchers. Our approach opens opportunities to study the functions of fundamentally important genes in specific contexts of plant development and creates the possibility of investigating postembryonic developmental processes.

RESULTS

Proof-of-Concept: Tissue-Specific GFP Knockout in the Lateral Root Cap

We reasoned that by using tissue-specific, somatic promoters to drive Cas9 expression, CRISPR could be used to generate cell-type-, tissue-, and organ-specific DNA mutations in plants. To test this hypothesis, we constructed T-DNA vectors with Cas9 expression controlled by the promoter region of *SOMBRERO/ ANAC033* (*SMB*). The *SMB* promoter (*pSMB*) is highly root-cap-specific and activated directly after the formative division of root cap stem cells (Willemsen et al., 2008; Fendrych et al., 2014). A *pSMB*:Cas9 expression cassette was combined with one of two gRNAs targeting the *GFP* coding sequence, GFP-1 and GFP-2, and transformed into a homozygous Arabidopsis line

with ubiquitous expression of a nuclear-localized GFP and β-glucuronidase (GUS) fusion protein (*pHTR5:NLS-GFP-GUS* [Ingouff et al., 2017]; henceforth, NLS-GFP). Primary transgenic plants (T1 seedlings) were selected via resistance to the herbicide glufosinate and investigated for loss of GFP signal in the root tips of 5 days after germination (DAG) seedlings. Six out of 11 *pSMB*:Cas9;GFP-1 events and three out of 10 *pSMB*:Cas9;GFP-2 events showed an almost complete loss of GFP specifically in the root cap, suggesting CRISPR-mediated knockout soon after the formative division of the root cap stem cells (Supplemental Figure 1A). All other root tissues maintained GFP expression, indicating that Cas9 activity specifically in the root cap cells led to cell-autonomous *GFP* knockout. The TSKO phenotype (de novo generation of mutations) was heritable, as T2 progeny from three lines with *pSMB*:Cas9;GFP-1 and three lines with *pSMB*:Cas9; GFP-2 had no GFP fluorescence in root cap cells while having normal NLS-GFP expression in all other tissues examined (Supplemental Figure 1B). These results indicate that the use of a tissue-specific promoter driving Cas9 can efficiently induce somatic TSKO phenotypes.

Design of the CRISPR-TSKO Gene Knockout Toolset

To facilitate a wide range of future gene-modification approaches in an easy-to-use cloning system, we devised CRISPR-TSKO, a modular and versatile vector toolset based on Golden Gate technology and modified GreenGate vectors (Engler et al., 2008; Lampropoulos et al., 2013). CRISPR-TSKO is inexpensive and immediately compatible with GreenGate modules already in use by other laboratories. The modularity allows for the combination of Cas9, or any nuclease, with virtually any promoter sequence of choice. Furthermore, it is possible to produce Cas9 fusion proteins on the N and C termini, allowing for the use of a wide range of

CRISPR technologies such as base editors (Marzec and Hensel, 2018) and transcriptional regulators (Lowder et al., 2015). The promoter, Cas9, N and C tags, and terminator modules can be combined with an "unarmed" gRNA cassette to generate an unarmed destination vector (Figure 1). One or two gRNAs can be directly cloned into this destination vector with a single Golden Gate reaction (see Methods). Alternatively, when a linker with AarI restriction sites is used instead of the unarmed gRNA cassette, a second round of Golden Gate assembly can be performed for the cloning of up to 12 gRNAs in a single destination vector (Supplemental Figure 2).

We generated a collection of binary destination vectors containing different selectable markers and/or nondestructive fluorescent markers based on the fluorescence-accumulating seed technology (FAST) system (Shimada et al., 2010) to take advantage of this general cloning strategy (Supplemental Data Set 1). The FAST system allows for the antibiotic- or herbicide-free selection of transformed T1 seeds and permits screening for phenotypes directly in T1 seedlings. To facilitate the evaluation of tissue specificity and expression levels of Cas9, we fused a nuclear-localized fluorescent mCherry tag to the *Cas9* coding sequence via a P2A ribosomal skipping peptide (Čermák et al., 2017). Using this Cas9-P2A-mCherry expression cassette (henceforth, Cas9-mCherry), we targeted different tissue types, cell lineages, and organs in Arabidopsis to explore the potential of CRISPR-TSKO for plant research.

Root-Cap-Specific Gene Knockout

To confirm the functionality of our vector system, the expression of Cas9-mCherry was controlled by *pSMB* and combined with the gRNA GFP-1. Ten of the 21 T1 seedlings (which expressed mRuby3 via the FAST system) showed a loss of GFP fluorescence
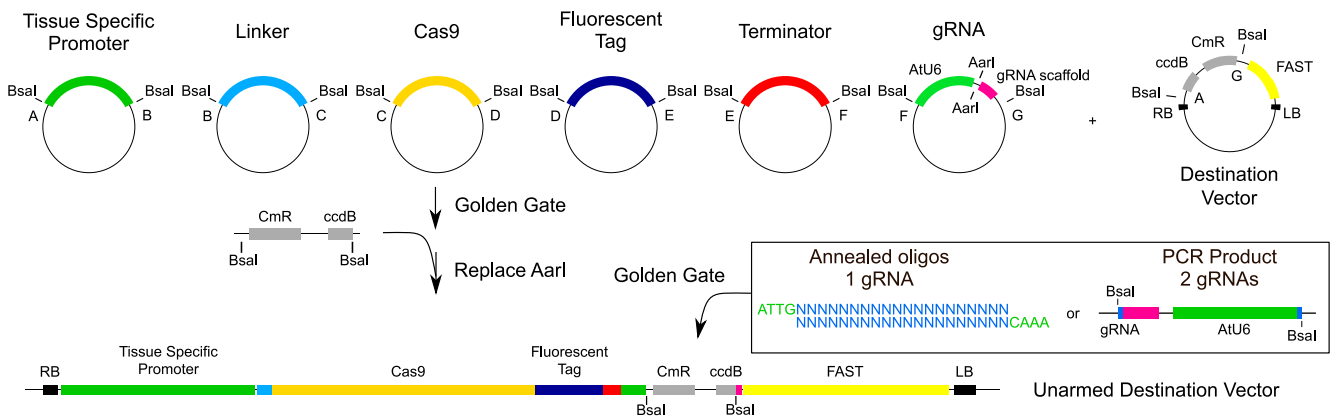

Figure 1. Cloning Workflow for CRISPR-TSKO Vectors.

Six entry modules are combined in a binary destination vector, containing a FAST screenable marker cassette, via Golden Gate assembly. The six entry modules contain a tissue-specific promoter, a cloning linker, the Cas9 nuclease, a fluorescent tag, a terminator, and a module containing an *AtU6-26* promoter driving the expression of an unarmed gRNA scaffold. These modules replace the *ccd*B and *Cm*R selectable markers, allowing for the negative selection of the destination vector in *ccd*B-sensitive *E. coli* cells. The resulting vector can be directly "armed" with one or two gRNAs upon predigestion with AarI. Alternatively, the AarI restriction sites can be replaced by a PCR product containing two BsaI sites flanking *ccd*B and *Cm*R expression cassettes. In a single Golden Gate reaction, a pair of annealed oligonucleotides are cloned, resulting in an expression vector containing one gRNA. Alternatively, Golden Gate cloning of a PCR product containing a first gRNA attached to an *AtU6-26* promoter and the spacer sequence of the second gRNA results in an expression vector containing two gRNAs.

specifically in the root cap, while six were chimeric (partial loss of GFP) and five maintained normal GFP expression (Figure 2A; Table 1). We observed a delay in the onset of the knockout phenotype, as cells of the youngest root cap layers had overlapping GFP and mCherry signals (Figure 2B). This suggests that a certain time for mRNA and/or protein turnover of GFP is required after the onset of Cas9 expression for the knockout phenotype to become apparent. We observed a clear correlation between the intensity of mCherry signal and the penetrance of the knockout phenotype: all ten highly expressing mCherry lines were entirely devoid of GFP signal in the root cap (except for the youngest cells), the medium-mCherry-expressing lines had chimeric knockout phenotypes, and the low- to no-mCherry lines had chimeric or full expression of GFP (Table 1). By comparing the intensity of both fluorescent proteins in individual root cap nuclei, we confirmed that highly expressing Cas9 lines had a significantly higher probability of gene knockout than the other lines (Figure 2C).

To test if a root cap-expressed gene, the NAC transcription factor *SMB* gene itself, could be successfully targeted by CRISPR-TSKO, we combined the gRNA GFP-1 with one of two different gRNAs targeting *SMB* (SMB-1 and -2) with Cas9 expression driven by *pSMB*. Loss of *SMB* delays root cap maturation and preparation for programmed cell death in root cap cells, leading to larger root caps and a delayed and aberrant root cap cell death with a lack of cell corpse clearance (Bennett et al., 2010; Fendrych et al., 2014). In T1 seedlings, we found *smb* mutant phenotypes for both SMB-1 and -2 coupled with the disappearance of root cap GFP signal (Supplemental Figure 3A). Both gRNAs appear to be equally effective, as 13 out of 21 and 9 out of 12 T1 events gave clear simultaneous *smb* and *GFP* knockout phenotypes, respectively (Table 2; Supplemental Figure 3A). Knockout phenotypes were scored in four segregating lines in the T2 generation. The *smb* and *GFP* knockout phenotypes were observed in all FAST-positive T2 seedlings, whereas all FAST-negative seedlings (null segregants) showed no knockout phenotypes (Figure 2D; Supplemental Figure 3B; Table 3). These data demonstrate that CRISPR-TSKO-induced mutations are strictly somatic when using *pSMB* and that the mutagenic effect is heritable.

To determine if the observed phenotypes were due to root-cap-specific DNA mutations, we prepared protoplasts from root tips of four independent T2 lines (two for each *SMB* target) and used them for fluorescence-activated cell sorting (FACS). DNA was extracted from sorted populations, and the *SMB* and *GFP* target loci were PCR amplified and Sanger sequenced. We performed TIDE analysis (Tracking of Indels by DEcomposition; Brinkman et al., 2014) to determine the frequency and type of knockout alleles generated. The mCherry-positive populations (Cas9-expressing) had indel frequencies (TIDE score) >95% for the GFP-1, SMB-1, and SMB-2 target loci (Supplemental Data Set 2). By contrast, the mCherry-negative cell populations had indel frequencies of 1 to 5%, which are equivalent to wild-type or background levels when using TIDE analysis. The alleles generated were largely consistent across events, with 1-bp insertions being the predominant outcome (58 to 94%) followed by 1-bp deletions (3 to 38%; Supplemental Data Set 2) for the GFP-1 target locus. A small but significant proportion of alleles were in-frame (3-bp deletions), but, as the GFP-1 gRNA targets the essential residue Gly67 (Fu et al.,

2015), these alleles likely result in no GFP fluorescence. For the two *SMB*-targeting gRNAs, 1-bp insertions were the predominant repair outcome (78 to 88%), with a minority (~10%) of alleles being 1-bp deletions for SMB-1 and 3-bp deletions for SMB-2 (Supplemental Data Set 2). Thus, the consistent *GFP* and *SMB* knockout phenotypes observed are due to active and heritable Cas9-induced somatic mutagenesis specifically in root cap cells.

Cell-Lineage-Specific Gene Knockout in the Stomatal Lineage

To test the possibility of using CRISPR-TSKO in a different somatic context, we utilized two promoter elements active in the stomatal cell lineage. The promoters of *TOO MANY MOUTHS* (*TMM*) and *FAMA* control gene expression in the stomatal lineage, with *pTMM* being expressed early in the lineage (Nadeau and Sack, 2002) and *pFAMA* being expressed later during the formation of guard mother cells and young guard cells (Ohashi-Ito and Bergmann, 2006). We used these two promoters to produce CRISPR-TSKO constructs simultaneously targeting *GFP* and *PHYTOENE DESATURASE3* (*PDS3*) in the stomatal lineage, as they should give clear knockout phenotypes. PDS3 is essential for chlorophyll, carotenoid, and gibberellin biosynthesis. Null mutants show a dwarfed and albino phenotype and cannot survive in soil (Qin et al., 2007). Consistent with this observation, the ubiquitously expressed Cas9-mCherry (*pPcUbi*:Cas9-mCherry; GFP-1,PDS3) gave rise to the expected severe phenotypic effects ranging from full albino to variegated leaves and stunted plants (Figure 3A; Supplemental Figure 4A).

Five days after germination, we assessed cotyledons of T1 seedlings for chlorophyll and GFP fluorescence by epifluorescence microscopy. Eighteen out of 20 *pTMM:*Cas9-mCherry; GFP-1,PDS-1 T1 seedlings were clearly lacking both GFP and chlorophyll fluorescence (Figure 3B), which is indicative of successful knockouts in both genes. In a separate experiment, two out of 23 T1 seedlings did exhibit some mild bleaching similar to the ubiquitous knockout events (Supplemental Figure 4A), suggesting that *pTMM* can drive Cas9-mCherry expression in mesophyll cells at a low frequency. Independent T2 *pTMM:*Cas9 plants were generally smaller than those of the NLS-GFP background line (Supplemental Figure 5) but were otherwise not affected in vegetative or reproductive development. Thus, restricting the loss of PDS3 to the stomatal lineage did not markedly affect plant development.

In contrast to the high frequency of *GFP* and *PDS3* knockout phenotypes in *pTMM*:Cas9-mCherry;GFP-1;PDS3 events, we observed neither a loss of GFP nor chlorophyll fluorescence in the 21 mCherry-expressing *pFAMA* T1 seedlings evaluated (Figure 3B). We hypothesized that *PDS3* and *GFP* mRNA and/or protein was persisting in the targeted cells due to the later induction of Cas9 by *pFAMA* and that these residual pools would have to be depleted before a loss of signal could be observed. Therefore, we investigated cotyledons 10 d after germination in five *pTMM*:Cas9 and eight *pFAMA*:Cas9 T1 events. Despite this extended cultivation time, mCherry-positive guard cells still showed clear GFP and chlorophyll fluorescence signals in the *pFAMA*:Cas9 lines (Supplemental Figure 4B).
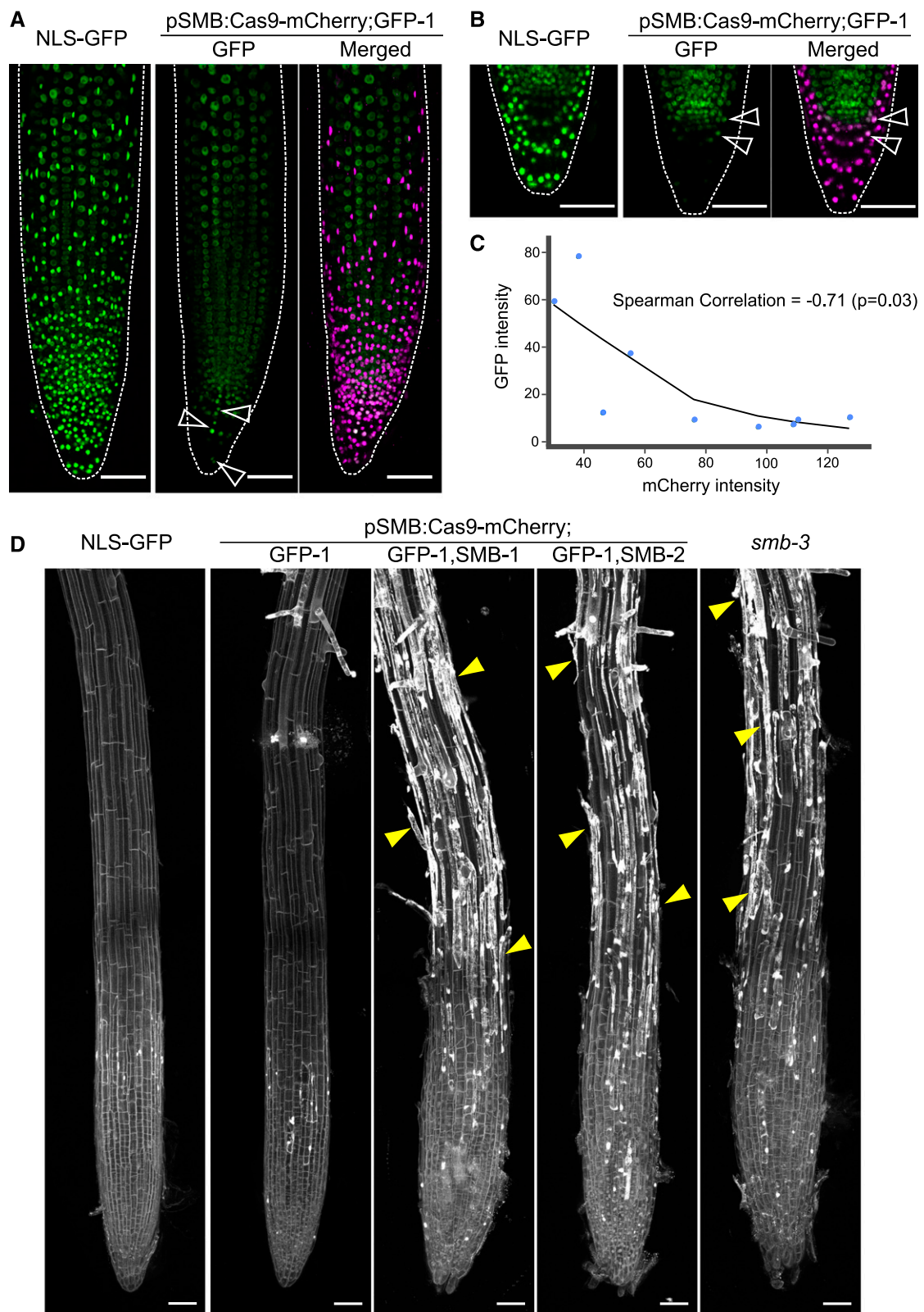
Figure 2. Root-Cap-Specific Knockout via CRISPR-TSKO.

To determine if DNA mutations were induced in both the *pTMM*:Cas9 and *pFAMA*:Cas9 lines, we prepared protoplasts from T2 cotyledons of two independent lines per genotype and sorted them for mCherry. Surprisingly, mCherry-positive cells from one *pFAMA*:Cas9 line (13,652.12) showed a reduced GFP fluorescence intensity during cell sorting (Supplemental Figure 6C). Genotyping of the mCherry-positive and -negative protoplast populations revealed an indel frequency of ~80% for the *GFP* and *PDS3* target loci for the *pTMM*:Cas9 lines and 30-74% for the *pFAMA:*Cas9 lines (Supplemental Data Set 3). The indel spectra for the *pTMM*:Cas9 line showed a preference for the 1-bp insertion. While the *pFAMA*:Cas9 lines had the same preference for the 1-bp insertion, they also had a greater variety of alleles, from 3-bp deletions to 2-bp insertions (Supplemental Data Set 3).

The detection of mutations in both *pFAMA*:Cas9 lines and the reduced GFP intensity detected by flow cytometry in one line was surprising given that a reduction of GFP signal was not observed by microscopy. To rule out technical errors, we performed a second sorting experiment on the two previously sorted *pFAMA*:Cas9 T2 lines plus two additional lines. From these four lines, we clearly observed indel frequencies of 23 to 75% for *GFP* and 34 to 86% for *PDS3* (Supplemental Data Set 4). Again, line 1365.12 had the highest indel frequencies and a reduction of GFP intensity (Supplemental Figure 7). The indel spectra were essentially identical to those of the first experiment, with 1-bp insertions being preferred for both *GFP* and *PDS3*. These results indicate that DNA mutations were generated in the mCherry-expressing cells for both CRISPR-TSKO constructs, but they do not resolve why knockout phenotypes were not observed in the *pFAMA*:Cas9 lines.

To determine if CRISPR-TSKO can be used to manipulate cell fate decisions within the stomatal lineage, we targeted *YODA* (*YDA*), a mitogen-activated protein kinase kinase kinase. Knockout mutants of *YDA* have clustered stomata, severe developmental defects, frequent seedling growth arrest, and, if they do manage to survive until flowering, sterility (Bergmann et al., 2004; Lukowitz et al., 2004). When we targeted *YDA* with a pair of gRNAs in a single, ubiquitously-expressed Cas9 construct (*pPcUbi*:Cas9-mCherry;YDA-1,YDA-2), 33 out of 35 mCherry-positive T1 seedlings contained clustered stomata on the cotyledonary epidermis to varying degrees of severity (Supplemental Figure 8A). Eight out of 19 T1 plants transferred to soil were sterile, which is consistent with the strong pleiotropic effects observed in reported *yda* mutants. When *YDA* was targeted by *pTMM*:Cas9-mCherry;YDA-1,YDA-2, all 40 T1 mCherry-positive seedlings had a clustered-stomata phenotype similar to that of the *yda-1* mutant,

Table 1. Phenotypes of T1 Seedlings Transformed with *pSMB*:Cas9-mCherry;GFP-1

mCherry	GFP Signal (n =21)		
	No	Chimeric	Normal
High	10	0	0
Medium	0	3	0
Low/no	0	3	5

yet without the corresponding growth arrest (Figure 3C; Supplemental Figure 8C). All 19 plants transferred to soil developed similarly to the wild type and were fertile.

PCR and DNA sequence analysis confirmed the efficient mutagenesis of *YDA* in T1 seedlings transformed with both *pPcUbi*:Cas9 and *pTMM*:Cas9 vectors. As a pair of gRNAs target *YDA*, an 813-bp deletion can be expected to occur via the excision of the intervening DNA sequence. Such deletion events were observed in events transformed with both vectors (Supplemental Figure 8B). Indel frequencies were higher for *pPcUbi*:Cas9 events than for *pTMM*:Cas9 events, as is expected for ubiquitous versus stomata-specific targeting (Supplemental Data Set 5). These results illustrate that by utilizing the stomatal lineage-specific *pTMM*, we are able to uncouple the pleiotropic growth defects and sterility in systemic *YDA* knockouts (Lukowitz et al., 2004) but still retain the characteristic clustered-stomata phenotype.

Organ-Specific Gene Knockout in Lateral Roots

After generating gene knockouts in particular tissues and cell lineages, we tested the potential of CRISPR-TSKO for generating mutant organs in otherwise wild-type plants. To this end, we made use of the previously published promoter sequence of *GATA23*, a gene that marks the onset of lateral root organogenesis and is expressed in pericycle cells primed to become involved in lateral root formation in Arabidopsis (De Rybel et al., 2010). *GATA23* expression is transient and disappears prior to the emergence of the primordium from the primary root, except for some remaining expression at the base of the primordium (Figure 4A; De Rybel et al., 2010). When targeting *GFP* with *pGATA23:*Cas9-mCherry;GFP-1, 20 out of 23 mCherry-positive T1 seedlings showed a complete or partial loss of GFP fluorescence in lateral roots while maintaining normal GFP expression in the primary root (Figures 4A and 4B; Table 4). By contrast, lines with undetectable mCherry expression showed chimeric or normal GFP expression in lateral

---

Figure 2. (continued).

(A) Maximum intensity projections of a representative NLS-GFP seedling and a *pSMB*:Cas9-mCherry;GFP-1 T1 seedling with the absence of GFP and presence of Cas9-mCherry signal specific to root cap cells. GFP is shown in green and Cas9-mCherry in magenta. Arrowheads indicate a patch of root cap cells in which GFP knockout was not achieved (chimera). All scale bars represent 50 μm.

(B) Midsections of root tips of an NLS-GFP seedling and a *pSMB*:Cas9-mCherry;GFP-1 T1 seedling. Arrowheads show young root cap cells in which GFP signal can still be observed. All scale bars represent 50 μm.

(C) Plot of median intensity of root cap nuclei for both GFP and Cas9-mCherry in T1 seedlings. Line shows a Loess regression curve.

(D) Overview of root tips of 6 DAG T2 seedlings for both gRNAs for SMB displaying the characteristic cell corpse accumulation at the root surface (yellow arrowheads) with propidium iodide staining.

Table 2. Phenotypes of T1 Seedlings Transformed with *pSMB*:Cas9-mCherry;GFP-1,SMB-1 and *pSMB*:Cas9-mCherry;GFP-1,SMB-2

Vector	mCherry	GFP Signal			*smb* Phenotype		
		No	Chimeric	Normal	Yes	Weak	No
GFP-1, SMB-1	High	12 (57%)	0	0	11 (52%)	1 (5%)	0
	Medium	3 (14%)	0	0	1 (5%)	2 (10%)	0
	Low	0	0	2 (10%)	0	0	2 (10%)
	No/very low	1 (5%)	1 (5%)	2 (10%)	1 (5%)	0	3 (14%)
GFP-1, SMB-2	High	8 (67%)	0	0	7 (58%)	0	1 (8%)
	Medium	0	0	0	0	0	0
	Low	0	3 (25%)	1 (8%)	2 (17%)	0	2 (17%)
	No/very low	0	0	0	0	0	0

roots (Table 4). Sequence analysis of lateral roots from six independent knockout events confirmed that >93% of the alleles were mutated in those organs (Supplemental Data Set 6). The indel spectrum was similar to those of the other tissue types, with the 1-bp insertion being the dominant repair outcome (Supplemental Data Set 6).

Knockout phenotypes were scored in three segregating lines in the T2 generation. For two lines, all FAST-positive plants had no GFP expression in the lateral roots, while in line 3, 15 out of 17 plants had no GFP expression in lateral roots (Table 5). Together, these experiments demonstrate that organ-specific gene knockout in lateral roots is highly efficient via the xylem-pole pericycle-expressed Cas9 controlled by *pGATA23*.

Lateral root organogenesis depends on the partially redundant action of *AUXIN RESPONSE FACTOR* (*ARF*) *7* and *ARF19*, as lateral root initiation is strongly inhibited in *arf7 arf19* double-knockout mutants (Okushima et al., 2007). As both *ARFs* are broadly expressed in Arabidopsis seedlings, it is unclear whether this phenotype depends on ARF7 and ARF19 function strictly in xylem-pole pericycle cells (Okushima et al., 2005). To test this hypothesis, we used CRISPR-TSKO with *pGATA23* to target both *ARF7* and *ARF19*. We first recapitulated the ubiquitous double-

knockout line *arf7 arf19* with two ubiquitously expressed Cas9 constructs, each containing two different gRNAs targeting both *ARFs* (*pPcUbi*:Cas9-mCherry;ARF7-1,ARF19-1 and *pPcUbi*:Cas9-mCherry;ARF7-2,ARF19-2). While no obvious reduction in lateral root density was observed in the T1 plants containing the first construct (*pPcUbi*:Cas9-mCherry;ARF7-1,ARF19-1), 18 out of 26 T1 plants containing the second construct (*pPcUbi*:Cas9-mCherry;ARF7-2,ARF19-2) completely lacked lateral roots (Supplemental Figure 9A), which is consistent with the phenotype of *arf7 arf19* seedlings (Okushima et al., 2005). In agreement with these phenotyping results, sequencing of the target loci in whole roots showed that the *pPcUbi*:Cas9-mCherry;ARF7-1,ARF19-1 construct was particularly ineffective, as the ARF19-1 target locus had an indel frequency of only 9 to 13% (Supplemental Data Set 7), explaining the lack of a mutant phenotype in those T1 plants. By contrast, the indel frequencies were >93% for most events with the *pPcUbi*:Cas9-mCherry;ARF7-2,ARF19-2 construct (Supplemental Data Set 7).

We quantified emerged lateral root density in three segregating T2 lines transformed with *pGATA23*:Cas9-mCherry;ARF7-2,ARF19-2. Slight but significant reductions in emerged lateral root density were observed in FAST-positive T2 plants (Figure 4C; Supplemental Figure 9B). As these results were inconsistent with those obtained using the ubiquitously expressed construct, we sequenced the *ARF7* and *ARF19* target loci in lateral roots of at least three plants per line. TIDE analysis revealed indel frequencies of >83% for ARF7-2 and >92% for ARF19-2 for nine out of 10 plants, and no wild-type alleles for either gene were detected in the lateral roots of four plants (Supplemental Data Set 8). Thus, lateral root initiation is only mildly affected when *ARF7* and *ARF19* are knocked out in *GATA23*-expressing pericycle cells.

Lateral-Root-Specific Knockout of Multiple CDKs Arrests Lateral Root Development

The central cell cycle regulatory gene *CYCLINE-DEPENDENT KINASE A1* (*CDKA;1*) is homologous to *CDK1* and *CDK2* in mammals. Cell proliferation is severely affected in *cdka;1* null mutants (Nowack et al., 2012). Mutant embryos are superficially normal in appearance but only contain a fraction of the number of cells that make up the wild-type embryo. Mutant seedlings are not viable in soil but can be cultivated as sterile dwarf plants without

Table 3. Segregating Phenotypes in T2 *pSMB*:Cas9-mCherry;GFP-1,SMB-1 and *pSMB*:Cas9-mCherry;GFP-1,SMB-2

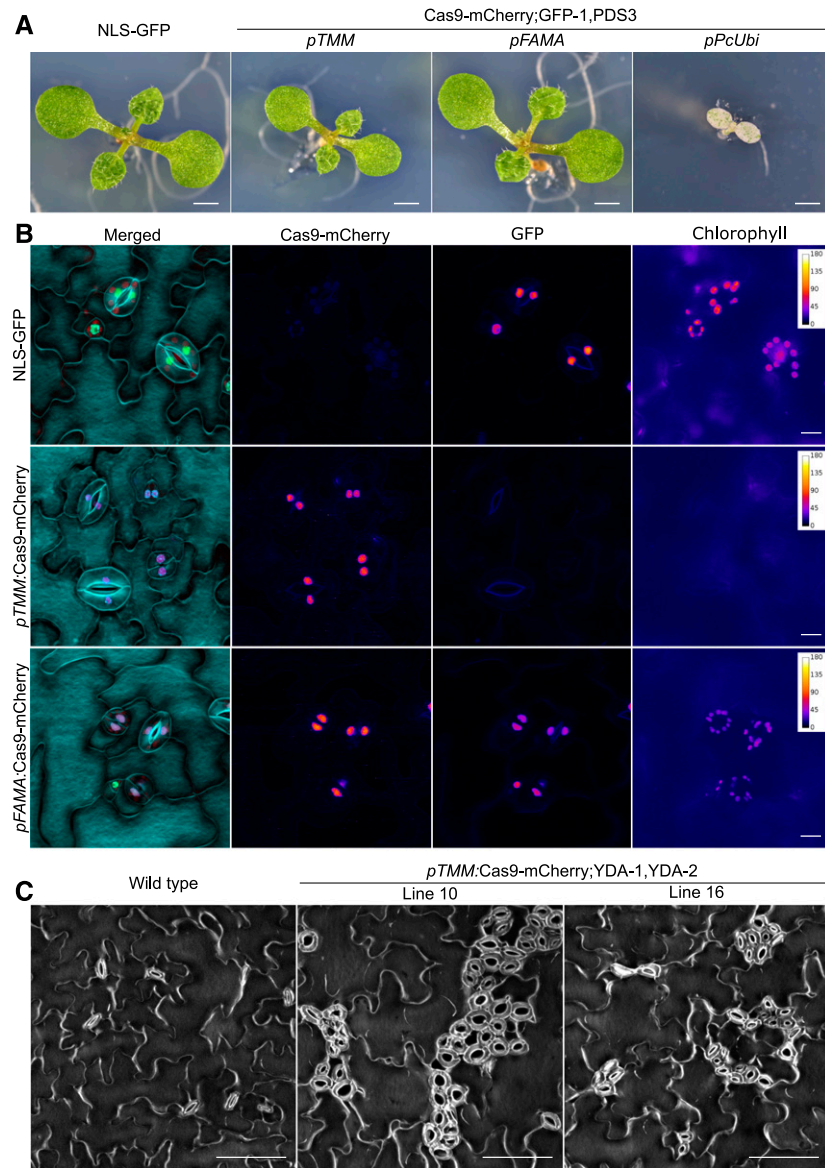| T1 line	FAST	n	mCherry		GFP Signal		*smb* Phenotype		
			+	−	No	Normal	Yes	Weak	No
GFP-1, SMB-1 line 2	+	34	34	0	34	0	33	1	0
	−	30	0	30	0	30	0	0	30
GFP-1, SMB-1 line 16	+	21	21	0	21	0	19	2	0
	−	30	0	30	0	30	0	0	30
GFP-1, SMB-2 line 12	+	30	30	0	30	0	29	1	0
	−	25	0	25	0	25	0	0	25
GFP-1, SMB-2 line 5	+	26	26	0	26	0	25	1	0
	−	33	0	33	0	33	0	0	33

Figure 3. Stomatal Lineage-Specific Knockout via CRISPR-TSKO.

(A) 9 DAG seedlings showing partial rescue when *PDS3* is knocked out only in the stomatal lineage (*pTMM*) compared with the arrested albino seedlings of the ubiquitous knockout line (*pPcUbi*). Scale bars represent 1 mm.

(B) Simultaneous stomata-lineage-specific knockout of GFP and chlorophyll biosynthesis in 5 DAG T1 seedlings. Shown are stomata at the abaxial faces of cotyledons. While both GFP and chlorophyll signals are lost in stomata in lines under the control of *pTMM*, signal is still present in stomata in lines under the control of *pFAMA*. In the merged images, cell outlines are in cyan, GFP in green, Cas9-mCherry in magenta, and chlorophyll fluorescence in red. Epidermal cell patterning is shown using DAPI staining. Scale bars represent 10 μm. Color bars on the right indicate fluorescence intensity (a.u.).

(C) Targeting of *YDA* only in the stomatal lineage (*pTMM*) is sufficient to cause clustering of stomata. Clusters of stomata are shown on the adaxial faces of cotyledons of 15 DAG T2 seedlings. Scale bars represent 100 μm.

a root system in axenic liquid cultures (Nowack et al., 2012). We generated CRISPR-TSKO constructs to specifically knockout *CDKA;1* in lateral root primordia to allow us to study the effect of CDKA;1 in the context of lateral root formation. We started by testing the efficiency of our gRNAs using ubiquitously expressed Cas9 with a paired-gRNA construct (*pPcUBI*:Cas9-mCherry; CDKA1-1,CDKA1-2). T1 seedlings reproduced the reported

dwarf-seedling phenotype (Nowack et al., 2012), and genotyping revealed a 171-bp deletion corresponding to the excision of the intervening DNA sequence (Supplemental Figure 10). TIDE analysis of the upper band showed higher indel frequencies with the gRNA CDKA1-1 (48 to 99%) than with the gRNA CDKA1-2 (16 to 79%; Supplemental Figure 10). The same gRNAs were also used with a *pGATA23* construct. All T1 transgenic plants grew
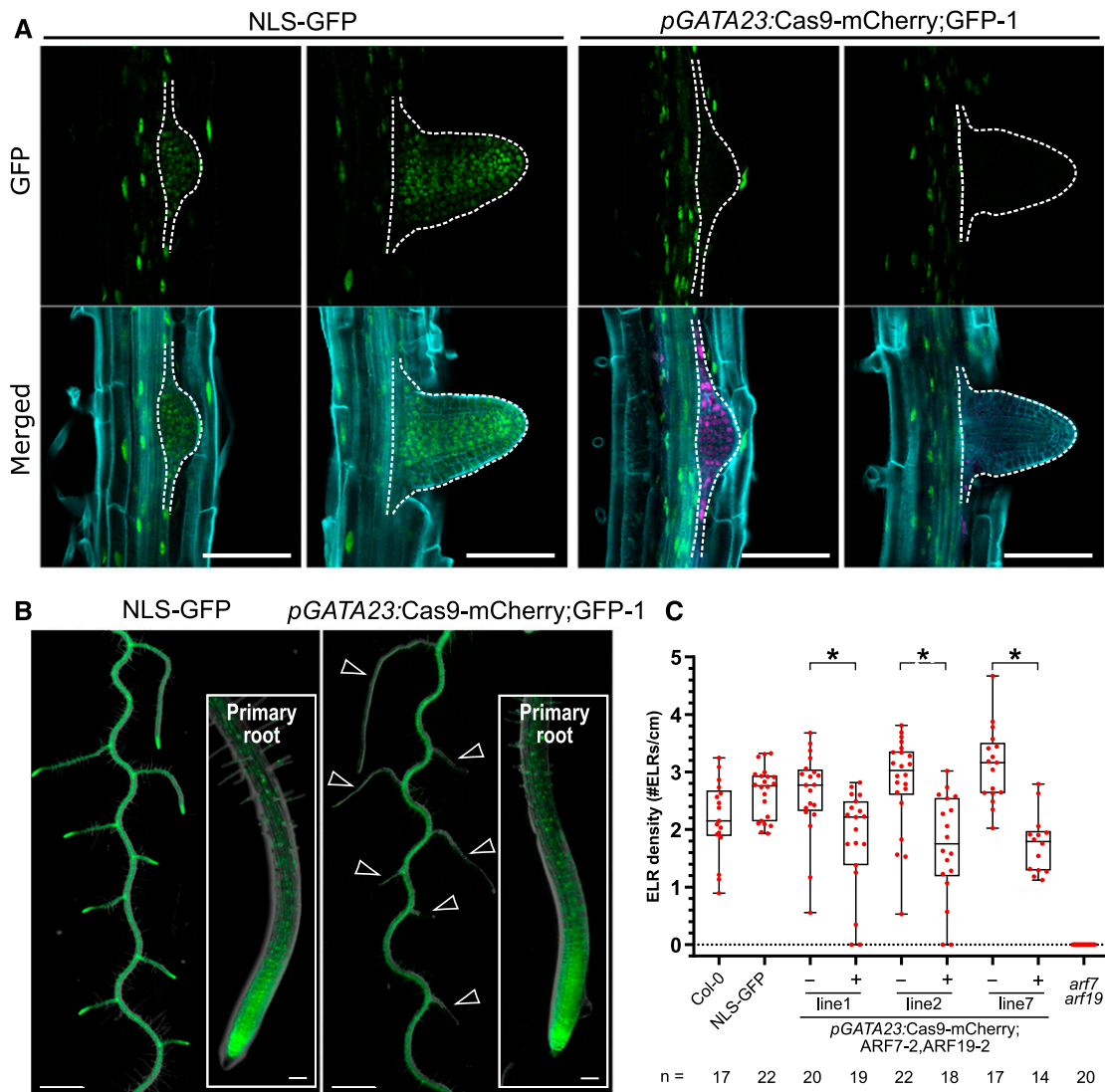
Figure 4. Organ-Specific Gene Knockout Using *pGATA23*-CRISPR-TSKO.

(A) Specific knockout of the GFP signal in emerging later roots (dashed outline). Representative images of the NLS-GFP control and *pGATA23*:Cas9-mCherry;GFP-1. GFP in green, mCherry in magenta, and cell wall stained with calcofluor white displayed in cyan. Scale bars represent 100 μm.

(B) GFP knockout is specific to lateral roots. Overlay of root morphology and GFP signal is shown for a representative NLS-GFP control and a T2 *pGATA23*:Cas9-mCherry;GFP-1 seedling. Arrowheads indicate GFP-negative lateral roots. Insets are the tip of primary roots. Scale bars represent 1 mm for overview and 100 μm for inset.

(C) Quantification of the emerged lateral root (ELR) density for Col-0 and FAST-positive (+) and -negative (−) T2 seedlings of *pGATA23*-CRISPR-TSKO lines targeting *ARF7* and *ARF19* simultaneously. The middle line of the boxplot indicates the median, the box indicates the lower and upper quartiles, and the whiskers indicate the minimum and maximum values. ELR density was compared between FAST positive and negative seedlings within each line via Poisson regression analyses. * indicates P values smaller than 2×10^{-3}.

normally and were fertile. In T2, we were surprised that lateral root development was not as severely affected as anticipated; lateral root density was unaffected and lateral roots of FAST-positive T2 plants were 62 to 69% the length of their null-segregant siblings (Figures 5A and 5C).

As the *CDK* gene family in Arabidopsis is composed of 10 partially redundant members (De Veylder et al., 2007), we hypothesized that the elimination of *CDKA;1* in lateral roots was being compensated for by the action of two B-type CDKs (*CDKB1;1* and *CDKB1;2*). In contrast to the *cdka;1* single mutant, *cdka;1 cdkb1;1* double mutants are embryo lethal, with embryo development arresting after a few rounds of cell division (Nowack et al., 2012). Therefore, we combined the gRNA CDKA1-1 with one of two different gRNAs that simultaneously target both *CDKB1* genes to generate triple knockouts (*pPcUBI*:Cas9-mCherry; CDKA1-1,CDKB1-1 and *pPcUBI*:Cas9-mCherry;CDKA1-1,CDKB1-

Table 4. GFP Phenotype in Lateral Roots of *pGATA23*:Cas9-mCherry;GFP-1

	GFP Signal in Lateral Roots		
mCherry	No	Chimeric	Normal
Positive	15	5	3
Negative	0	3	27
Total seedlings	15	8	30

2). If the vectors were effective, we expected severe seedling phenotypes or even failure to recover FAST-positive T1 seeds. Indeed, the few FAST-positive T1 seedlings we could recover showed severe developmental defects, and many died in axenic culture (Supplemental Figure 11). We were able to isolate DNA from some of these seedlings and confirmed that the indel frequencies were >90% for all three genes in four out of seven independent *pPcUBI*:Cas9-mCherry;CDKA1-1,CDKB1-1 lines (Supplemental Figure 11; Supplemental Data Set 9). The second *CDKB1* gRNA was less effective, as most events had indel frequencies of only ~20 to 70%. It is important to note that due to the severe growth defects in these mutants, we observed a negative selection pressure against events transformed with *pPcUBI*:Cas9-mCherry;CDKA1-1,CDKB1-1 (Supplemental Figure 12), and many of the most severely affected plants did not yield sufficient DNA for genotyping. Nevertheless, these results indicate that both gRNAs are effective, with the CDKB1-1 gRNA being more efficient.

We next generated triple *CDK* lateral root knockouts using a *pGATA23* construct. Macroscopically, the transgenic lines exhibited an apparent lack of lateral roots (Figure 5A). However, upon closer inspection, we found that lateral roots did form, but they arrested growth soon after emergence (Figures 5B and 5D). These stunted lateral roots showed the characteristic reduced number of cells and the presence of grossly enlarged epidermal and cortex cells in mutants severely affected in cell cycle progression (Nowack et al., 2012). Furthermore, we detected a slight but significant reduction in emerged lateral root density in FAST-positive segregants in three independent lines (Figure 5C), suggesting that some lateral roots did arrest before emergence.

DISCUSSION

CRISPR-TSKO of Essential Genes Enables Their Study in Specific Contexts

Targeted gene knockout experiments in plants typically have the objective of generating inheritable mutant alleles that will be transmitted to the offspring. The generation of such knockout lines is a powerful tool for the functional analysis of many genes of interest. However, this approach is difficult to apply to genes that are essential for cell survival, reproduction, or those that have severe pleiotropic effects when mutated. Moreover, the context

specificity of key regulators in developmental processes is often assumed by researchers, without experimental proof, while being aware of their non-context-specific expression. In this report, we describe the design and validation of CRISPR-TSKO, a tissue-specific gene knockout approach in plants that can be used to overcome these limitations.

In total, we targeted nine genes using four different tissue-specific promoters. Several of the target genes (*PDS3*, *YDA*, *CDKA;1*) are essential for plant growth, development, and/or reproduction. Mutations in *PDS3* induced by *pTMM*:Cas9-mCherry;GFP-1;PDS3 led to the expected defects in chlorophyll content and chloroplast formation (Qin et al., 2007) specifically in the stomatal lineage. Importantly, the active photosynthetic mesophyll tissue was not markedly affected in non-Cas9-expressing cells, which allowed these plants to develop similarly to the wild type. This stands in contrast to the ubiquitous CRISPR knockout plants, which were primarily dwarfed, albino and not viable in soil (Figure 3A; Supplemental Figure 4A).

In wild-type Arabidopsis, chlorophyll-containing chloroplasts form in epidermal pavement cells as well as stomatal guard cells, although they are much smaller than mesophyll chloroplasts (Barton et al., 2016). The function of chloroplasts in guard cells has been the subject of debate (Lawson, 2009). Recently, the discovery of the Arabidopsis *green less stomata 1* mutant further supports the hypothesis that functional chloroplasts in guard cells are important for stomatal responses to CO_2 and light, resulting in stomatal opening (Negi et al., 2018). CRISPR-TSKO plants with mutated *PDS3*, or other genes required for chloroplast development and/or function, specifically in the stomatal lineage can be powerful tools to test these and other hypothesized functions of chloroplasts in guard cells.

The mitogen-activated protein kinase YDA has a plethora of roles during plant development including embryogenesis, epidermal patterning, and root development (Musielak and Bayer, 2014; Smékalová et al., 2014). Accordingly, *yda* mutants have severe pleiotropic phenotypes. Soon after fertilization, *yda* mutants fail to establish the first asymmetric division of the zygote,

Table 5. Phenotypic Analysis of T2 Seedlings of *pGATA23*:Cas9-mCherry;GFP-1

T1	FAST	n	mCherry		GFP in LR	
			+	−	No	Normal
Line 1	+	16	16	0	16	0
	−	10	0	10	0	10
Line 2	+	7	7	0	7	0
	−	18	0	18	1[a]	17
Line 3	+	17	17	0	15	2
	−	20	0	20	0	20

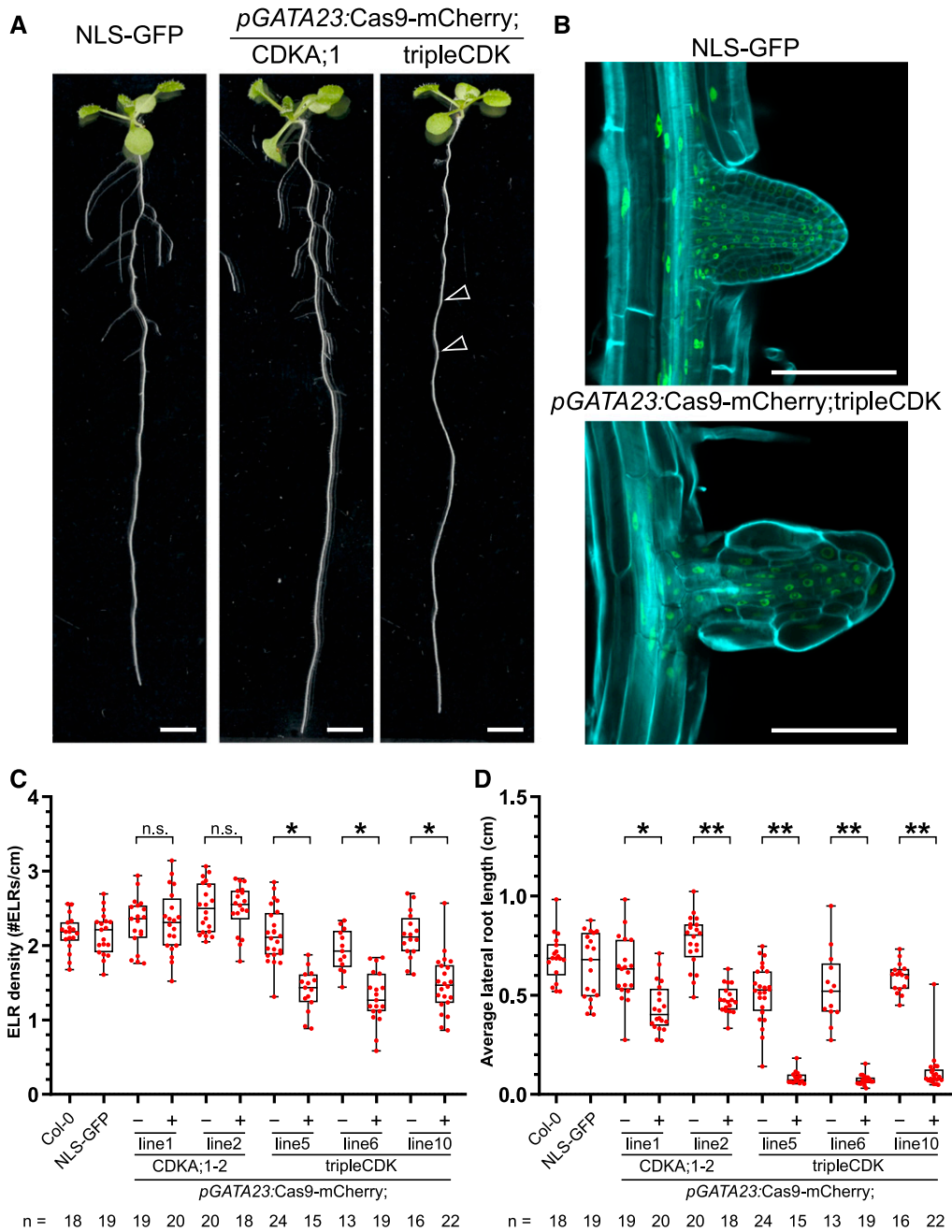[a]Plant showed no GFP signal in the entire plant.

Figure 5. Lateral-Root-Specific Gene Knockout of Cell Cycle Regulators Using p*GATA23*-CRISPR-TSKO.

(A) Representative 12 DAG seedlings of NLS-GFP, T2 seedling of *pGATA23*:Cas9-mCherry;CDKA;1-1,CDKA;1-2, and T2 seedling of *pGATA23*:Cas9-mCherry;CDKA;1-2,CDKB1-1 (tripleCDK). Arrowheads show emerged lateral roots with an extremely reduced cell number. Scale bars represent 0.5 cm.
(B) Confocal images of an emerged lateral root in NLS-GFP and *pGATA23*:Cas9-mCherry;tripleCDK. GFP in green and cell wall stained with calcofluor white displayed in cyan. Scale bars represent 100 μm.
(C) Quantification of the emerged lateral root (ELR) density of Col-0, NLS-GFP, and FAST negative (−) and positive (+) T2 seedlings of *pGATA23*-CRISPR-TSKO lines targeting either *CDKA;1* or *CDKA;1*, *CDKB1;1*, and *CDKB1;2* simultaneously. The middle line of the boxplot indicates the median, the box indicates the lower and upper quartiles, and the whiskers indicate the minimum and maximum values. ELR density was compared between FAST positive and negative seedlings within each line via Poisson regression analyses. n.s. indicates not significant with an $\alpha = 0.05$. * indicates P values smaller than 4×10^{-4}.
(D) Quantification of average lateral root length of same seedlings as in **(C)**. The middle line of the boxplot indicates the median, the box indicates the lower and upper quartiles, and the whiskers indicate the minimum and maximum values. A random-effects model was used to estimate the effect of CRISPR-TSKO on the lateral root lengths between FAST positive and negative seedlings within each line. * indicates P values smaller than 6×10^{-3}; ** indicates P values smaller than 1×10^{-4}.

and ensuing embryo development is severely compromised (Lukowitz et al., 2004). Some *yda* embryos do continue to develop into seedlings, but these rarely survive in soil, and the few *yda* plants that flower are severely dwarfed and completely sterile (Bergmann et al., 2004; Lukowitz et al., 2004). While loss-of-function *yda* lines can be maintained in a heterozygous state, previous reports and our own experience show that only a small proportion of homozygous seedlings can be obtained due to germination issues or very early seedling lethality (Lukowitz et al., 2004). This low recovery rate poses a considerable obstacle when designing and conducting experiments.

Using CRISPR-TSKO to target *YDA* only in the stomatal lineage, all transgenic events expressed a range of clustered-stomata phenotypes, while other aspects of plant development were not notably compromised. Critically, all lines transferred to soil were fertile and we were able to generate normally segregating T2 populations. These results demonstrate that by using CRISPR-TSKO, we are able to uncouple the pleiotropic defects caused by *YDA* mutations to study its functions in the stomatal lineage.

The specific cellular defects caused by mutations in essential genes such as central cell cycle regulators are challenging to investigate due to lethality in the gametophyte or embryonic stage, and accordingly, low transmission rates (Nowack et al., 2012). CRISPR-TSKO enabled us to generate presumably higher-order *CDK* mutant lateral roots with striking cell proliferation defects on otherwise wild-type plants. These mutant plant lines offer a convenient opportunity to investigate the cellular defects caused by depletion of CDK proteins in an easily accessible tissue in the T1 or later transgenic generations. Interestingly, cell proliferation in the stele of triple-CDK lateral roots appeared to be less affected than in the epidermis and cortex. Whether this is caused by the differential turnover of CDK mRNA and/or proteins in different cell types or by the differential requirement of CDK activity in different tissues remains to be tested. Depletion of the CDKA;1 target RETINOBLASTOMA-RELATED1 (RBR1) has been shown to attenuate the cell proliferation defect in *cdka;1* mutants (Nowack et al., 2012), suggesting that tissue-specific differences in gene expression levels might contribute to differential responses to the loss of CDK function. Alternatively, other CDK classes might be able to partly compensate for CDKA and CDKB loss of function in specific cell types (Inze and De Veylder, 2006). These different scenarios could be addressed by CRISPR-TSKO in the future. Similarly, many other central cell cycle or cell division regulators, of which no homozygous plants can be recovered, become amenable for detailed cellular investigation by CRISPR-TSKO.

Generation of Entire Mutant Organs with CRISPR-TSKO

To generate entire mutant organs on otherwise wild-type plants, we targeted primordial founder cells responsible for the generation of the root cap and whole lateral roots. The root cap is an organ that covers and protects the stem cells at the root tip. Although the root cap has relatively low tissue complexity, it encompasses many aspects of plant development—generation by stem cells, proliferation, differentiation, and finally programmed cell death—in a compact spatial and temporal frame of a few hundred micrometers and a couple of days (Kumpf and Nowack, 2015). SMB is a key transcription factor required for root cap maturation and

programmed cell death, and its expression starts immediately after the formative stem cell division in root cap daughter cells (Willemsen et al., 2008; Fendrych et al., 2014). We showed that even an early acting gene such as *SMB* itself can be efficiently targeted, thereby affecting root cap development. In this model system, the *pSMB*-CRISPR-TSKO vector toolkit could be particularly useful for studying genes essential for basic cellular functions in this easily accessible, nonessential root organ.

Lateral roots arise from a subset of stem cells situated in the pericycle at the xylem poles. These cells express *GATA23*, a gene that marks the onset of lateral root organogenesis, and undergo tightly coordinated asymmetric cell divisions to generate cell diversity and tissue patterns, resulting in the development of a lateral root primordium (De Rybel et al., 2010). By targeting *GATA23*-expressing pericycle cells, we were able to generate plants with entirely mutated lateral roots. The generation of completely GFP-negative lateral roots in 87% of T1 events demonstrates the high efficiency of CRISPR-TSKO under the regulatory control of *pGATA23*. Having a promoter at hand that is activated in the precursor cells of a new organ thus represents an effective means to generate whole organs devoid of the function of a gene of interest. Thus, the use of CRISPR-TSKO may be an attractive alternative to grafting in certain experimental systems without the tedious process of generating a graft junction. In addition, novel arrangements of genotypes that would not be practical or possible using grafting can now be generated within an individual plant. Moreover, essential genes for primary root development such as *MONOPTEROS* hinder loss-of-function analysis during lateral root development (De Smet et al., 2010). The *pGATA23*-CRISPR-TSKO system will enable us to uncouple the functions of such genes involved in primary and lateral root development.

Auxin signaling is essential for lateral root initiation and development. The auxin response factors ARF7 and ARF19 are required for the auxin-induced pericycle cell divisions that constitute a lateral root initiation event. These divisions are strongly inhibited in *arf7 arf19* double-knockout mutants, which hardly produce any lateral roots (Okushima et al., 2007; Lavenus et al., 2013). *ARF7* is expressed in the initials of the vasculature and pericycle cells starting from the elongation zone, while *ARF19* is much more broadly expressed in the primary root (Okushima, 2005; Rademacher et al., 2011). Given their expression beyond the cells that actually contribute to lateral root formation, it has so far remained unresolved whether the role of ARF7 and ARF19 in lateral root initiation depends strictly on their activity in xylem-pole pericycle cells. Interestingly, targeted mutagenesis of *ARF7* and *ARF19* using *pGATA23* does not result in the strong inhibition of lateral root initiation, as observed in *arf7 arf19* seedlings (Figure 4C).

This observation suggests that the function of ARF7 and ARF19 in lateral root precursor cells is not essential for lateral root development and that their activity is required before the initiation of lateral root organogenesis and thus prior to the activation of *pGATA23*, or even in another tissue. This raises the question of when and in which cells of the primary root these ARFs are necessary for lateral root development. Alternatively, ARF7/ARF19 mRNA and/or protein may persist in *GATA23*-expressing cells long enough to promote lateral root initiation. To test these hypotheses, we will be able to utilize CRISPR-TSKO with different

promoters with unique spatiotemporal expression patterns. Furthermore, the use of fluorescently tagged translational fusion ARF7/ARF19 lines will allow us to track their depletion upon CRISPR-TSKO targeting and establish the precise developmental window of ARF7/ARF19 signaling necessary for lateral root initiation.

CRISPR-TSKO: A Powerful and Versatile Tool

We developed a modular vector-cloning scheme based on the GreenGate system (Lampropoulos et al., 2013) to facilitate the construction of CRISPR-TSKO reagents. The modularity of the cloning system allows for the rapid assembly of new promoter sequences with Cas9 or any nuclease of choice. To further enable the use of this technology, we developed a Cas9-P2A-mCherry; GFP-1 destination vector (pFASTR-BsaI-*Cm*R-*ccd*B-BsaI-Cas9-P2A-mCherry-G7T-AtU6-GFP-1) with an empty promoter module containing a *ccd*B/*Cm*R cassette flanked by BsaI restriction sites. Any promoter in a GreenGate entry vector can be inserted into this destination vector with a single Golden Gate reaction, and researchers can immediately test the suitability of their promoter for CRISPR-TSKO in a GFP-expressing background line. Targeting in specific spatial and temporal contexts can also be readily achieved using inducible and tissue-specific plant expression systems that utilize GreenGate technology (Schürholz et al., 2018).

The cloning reagents used here are inexpensive, require minimal hands-on time, and can be readily adopted by any laboratory. The system can currently accommodate up to 12 gRNAs by the use of an AarI linker and additions of six paired-gRNA entry modules (Supplemental Figure 2; Supplemental Protocol). By recycling the AarI-linker, it is possible to clone even more gRNAs. For ease of use, a workflow was developed to substitute the AarI restriction sites in the linker for BsaI restriction sites flanking the *ccd*B and *Cm*R selectable markers (Figure 1; Supplemental Figure 2; Supplemental Protocol). This strategy avoids the need for separate AarI digestions of regularly used destination vectors and provides a negative selection marker for the original destination vector in *ccd*B-sensitive *Escherichia coli* cells (e.g. DH5α). Alternatively, additional expression cassettes can be sequentially inserted into the AarI-*Sac*B or BsaI-*ccd*B linkers. Hence, the system presented here can be easily used and modified for a variety of genome-engineering applications such as transcriptional regulation (Lowder et al., 2015) and base editing (Marzec and Hensel, 2018).

Considerations for the Use of CRISPR-TSKO

One general characteristic of CRISPR-TSKO is the continuous de novo generation of mutations in cells that start to express Cas9. In the case of the root cap, every newly generated root cap cell starting to express SMB can create a novel gene knockout event. In the stomatal lineage, every cell that starts expressing TMM or FAMA generates independent lineages, and in the case of the lateral root, every *GATA23*-expressing founder cell will contribute individual mutations to the lateral root primordium (von Wangenheim et al., 2016). Therefore, unlike in ubiquitous, inheritable

mutant approaches, no defined mutant alleles are generated. Most mutations are small (1 to 3 bp) indels causing frame shifts and early stop codons, but, depending on the gRNA, some will also lead to in-frame missense mutations. Despite this source of variation, we were able to observe knockout phenotypes of varying degrees for all of the genes investigated. Furthermore, DNA repair outcomes from Cas9-mediated cleavage are nonrandom (Allen et al., 2018). Indeed, mutation analysis of the CRISPR-TSKO events showed that gRNAs largely give the same indel spectrum regardless of the tissue-specific promoter used. For example, the most common indel generated for the GFP-1 target locus in *SMB*-, *TMM*-, *FAMA*-, and *GATA23*-expressing cells is a 1-bp insertion, followed by 1- and 3-bp deletions (Supplemental Data Sets 2 to 4, and 6). The continuous generation of indels does present one general limitation to CRISPR-TSKO, in that crossing of well-defined and characterized mutant lines to generate higher-order mutants, a common practice with stable knockouts, might not be advisable here, as there could be silencing of the stacked T-DNAs and inefficient generation of indels after a cross. Instead, if higher-order TSKOs are desired, we recommend generating new transgenic lines from multi-gRNA vectors or using a combination of stable mutant alleles and CRISPR-TSKO. Researchers can first establish a stable higher-order mutant and check for phenotypes. If pleiotropic and lethality issues are encountered, the highest-order mutant that does not have a problem can be used with CRISPR-TSKO to generate tissue-specific phenotypes without pleotropic effects.

Some gRNAs do not induce mutations at high efficiency. The ARF7-1 and ARF19-1 gRNAs are a clear example of this, with ARF7-1 giving indel frequencies of 20 to 60% and ARF19-1 giving only 3 to 13%. These low indel frequencies are the most likely reason for the lack of a lateral root phenotype in the ubiquitously expressed Cas9 T1 plants. Based on this finding and the observation that indel outcomes are nonrandom, we recommend that users of CRISPR-TSKO initially generate multiple gRNAs to target genes of interest, as we have done in most of the experiments reported here. In cases where the targeted cells will be of low abundance (only a few cells targeted, e.g. *pSMB*, or knockout of essential genes, e.g. *CDKA;1*), making it challenging to obtain sufficient material for genotyping, controlling Cas9 expression with a ubiquitous promoter such as *PcUbi* or *GATA23* (to generate mutant lateral roots) is a reasonable way to test the efficiency of a gRNA. This experiment could also establish whether a gene is essential when an efficient gRNA is identified.

Users should also consider targeting functional domains, as is generally recommended with any standard knockout strategy. For example, the gRNA GFP-1 used here targets the essential Gly67 residue for GFP fluorescence, so that even in-frame mutations result in a loss of fluorescence (Fu et al., 2015). Hence, the use of gRNAs targeting genes of interest in particularly sensitive sites, such as crucial interaction domains or active sites, could further increase the likelihood of CRISPR-TSKO being effective.

We observed a strong correlation between gene knockout and Cas9-mCherry expression, which could be used to facilitate event selection. Furthermore, targeting of *GFP* alongside a gene of interest in a ubiquitously expressing NLS-GFP background revealed that knockout of GFP strongly correlated with mutagenesis of the endogenous genes *SMB* and *PDS3*. Thus, the use of both

tagged Cas9 and knockout of reporter genes could facilitate the selection of successful knockout events in tissues and organs. While the loss of GFP signal should not be taken as definitive proof that the function of a gene of interest is also lost, it allows for an easy readout when testing CRISPR-TSKO in new cell types and developmental contexts.

Limitations of CRISPR-TSKO

Depending on the promoter used or gene targeted, CRISPR-TSKO experiments might not always be straightforward. This is illustrated by our use of the *pFAMA* promoter sequence. While we initially were unable to observe an obvious microscopic pheno-type when targeting *GFP* and *PDS3*, we did observe a reduced GFP signal by flow cytometry for one transgenic line, and DNA mutations were detected in all four sorted lines. Therefore, Cas9 expression in these cells led to DNA mutations (albeit, at a lower frequency than other experiments) but conferred only a modest phenotypic effect. If indels are generated via independent events and given the indel frequencies we observed (23 to 75%; Supplemental Data Set 4), we would expect ~5 to 56% of the guard cells to be knocked out for GFP. However, guard cells completely lacking GFP expression were not observed in our *pFAMA* experiments. In our experiments with *pSMB*, residual GFP fluorescence was detectable in the two youngest root cap layers, with some overlap between mCherry and GFP signals (Figures 2A and 2B). Therefore, we hypothesize that mRNA and/or protein turnover is required before knockout phenotypes can be ob-served. The speed of these processes likely depends of the stability of the particular mRNA and protein, and, considering our *pFAMA* observations, might also depend on the cell type in question. The negative results presented here highlight the notion that these dynamics should be considered on a gene-by-gene and tissue-specific promoter basis when designing and analyzing CRISPR-TSKO experiments.

Our results indicate that choosing the right promoter is critical for the success of a CRISPR-TSKO experiment. A collection of GreenGate-based, tissue-specific promoters was recently de-scribed and is a good starting point for users to test new promoter elements (Schürholz et al., 2018). With the recent adoption of single-cell RNA sequencing for plant research (Denyer et al., 2019), the list of tissue-specific promoters will continue to grow and develop. Despite these extensive lists of tissue-specific promoters that are available, it is still unclear how to accurately predict which promoters will be most effective. With our results showing that higher Cas9 expression is correlated with more efficient gene knockout, it is tempting to speculate that a strong promoter would be beneficial. However, we have not directly tested predicted promoter strength and knockout efficiency. Therefore, we recommend that users empirically test the effec-tiveness of a promoter before conducting more extensive studies. This test could simply be performed by analyzing the ubiquitously expressing NLS-GFP (NASC ID N2109788) line transformed with the highly efficient gRNA GFP-1 under the control of a new pro-moter of choice. Alternatively, translational fluorescent fusion lines could be used to monitor the elimination of a protein of in-terest from a particular cell type.

Alternative approaches to eliminate gene products in specific cells, tissues, or organ types typically rely on the use of gene silencing. Tissue-specific or inducible RNAi, either through the use of artificial miRNAs (Alvarez et al., 2006; Schwab et al., 2006) or hairpin vectors (Burgos-Rivera and Dawe, 2012) have been used to specifically silence genes in a tissue-dependent or transient manner. Importantly, the mechanisms for gene silencing and DNA mutagenesis are distinct, and each presents its own tradeoffs. Perhaps the most significant difference is that gene silencing does not completely eliminate RNA and the degree of silencing can be gene dependent (Kerschen et al., 2004). This permits low levels of gene expression and gene effects to be overlooked in cases where the mRNA and/or protein are very stable or are required in only minute amounts. At the same time, this has also been regarded as an advantage, as it allows for the continued growth and development of plant tissues when the targeted gene is essential for basic cellular functions. By contrast, CRISPR-mediated mu-tagenesis leads to the complete elimination of gene products, except in specific cases (e.g. *pFAMA*:Cas9). This feature should enable the observation of more precise and striking phenotypes. However, researchers need to carefully consider how the absence of mutant cells (when targeting essential genes) might affect their downstream analysis. For example, in our own experiments, the knockout of the CDKs in lateral roots prevented us from obtaining sufficient material to confirm DNA mutagenesis in the affected lateral roots.

Both systems have the potential for inducing off-target effects. While a systematic comparison between RNAi and CRISPR-mediated knockout in plants has not been reported, a recent large-scale gene expression profiling study with mammalian cell lines comparing CRISPR and RNAi found that the off-target ef-fects of RNAi are much greater than typically anticipated. As our understanding of the on- and off-target parameters of gRNA design increases, CRISPR technology could be employed with negligible off-target activity (Smith et al., 2017). But again, off targets can be useful when targeting gene families with either RNAi (Hauser et al., 2013) or CRISPR (Endo et al., 2015).

One inherent limitation to the CRISPR-TSKO approach is that it requires stable transformation and expression of Cas9 and the gRNA(s). Therefore, this technique has the same constraints as any standard transgenic approach, in that the plant species or variety must be transformable and that sufficient independent events can be obtained to identify those with stable and consistent transgene expression over generations. Virus-induced gene si-lencing has been used for crop plants that are recalcitrant to transformation (Senthil-Kumar and Mysore, 2011). However, as the silencing effect is reliant on the spread of the virus particles throughout the plant, the effect is nonuniform and is rarely used in a tissue-specific manner (Kushwaha and Chakraborty, 2017). To address the issue of selecting lines with consistent transgene expression, the vectors developed here contain mCherry-NLS transcriptionally fused to Cas9, which easily enables the identi-fication of lines with stable Cas9 expression.

In conclusion, cell-type-, tissue-, or organ-specific gene knock-out by targeted expression of Cas9 is a powerful method for functional genetic analysis in specific spatial and temporal con-texts of plant development. This is especially true for genes that are widely expressed or have fundamental roles in cell survival or

plant reproduction. CRISPR-TSKO allows for the rapid generation of stable transgenic lines with de novo somatic DNA mutations specific to the cell, tissue, or organ of interest. Due to its flexibility and ease of use, we foresee this tool as enabling the discovery of context-specific gene functions. Moreover, the scalability of the system allows for quick initial investigation of candidate genes with the reduced influence of pleiotropic effects. As with other CRISPR applications, CRISPR-TSKO is forward compatible to incorporate upcoming future variations of CRISPR gene modification. Together with the virtually unlimited possibilities to combine different promoters, reporters, or tags in CRISPR-TSKO, this technology represents a powerful addition to the molecular genetics toolbox for plant biology research.

Distribution of Plant Lines, Plasmids, and Protocols

All cloning modules and plasmids reported here are available via the VIB-UGent Center for Plant Systems Biology Gateway Vector website (Supplemental Data Set 1; http://gateway.psb.ugent.be/search) or via Addgene (http://www.addgene.org/). See Supplemental Protocol for detailed cloning protocols.

METHODS

Cloning

All cloning reactions were transformed via heat-shock transformation into *ccd*B-sensitive DH5α *Escherichia coli* or One Shot *ccd*B Survival 2 T1R Competent Cells (Thermo Fisher Scientific). Depending on the selectable marker, the cells were plated on LB medium containing 100 μg/mL carbenicillin, 100 μg/mL spectinomycin, 25 μg/mL kanamycin, or 10 μg/mL gentamycin. Colonies were verified via colony-touch PCR, restriction digestion, and/or Sanger sequencing by Eurofins Scientific using the Mix2Seq or TubeSeq services. All PCR for cloning was performed with Q5 High-Fidelity DNA Polymerase (New England Biolabs) or iProof High-Fidelity DNA Polymerase (Bio-Rad Laboratories). Gibson assembly reactions were performed using 2× NEBuilder Hifi DNA Assembly Mix (New England Biolabs). Column and gel purifications were performed with Zymo-Spin II columns (Zymo Research).

Golden Gate Entry Modules

Golden Gate entry modules were constructed by PCR amplification of gene fragments and inserting the purified PCR product into BsaI-digested GreenGate entry vector (Lampropoulos et al., 2013) via restriction-ligation using BsaI (New England Biolabs) or Gibson assembly. See Supplemental Data Set 10 for all primers used. All generated clones were verified via Sanger sequencing.

The coding sequence for mTagBFP2, based on a previously reported mTagBFP2 (Pasin et al., 2014), was PCR amplified with primers RB42 and RB43 from a synthesized fragment (Gen9) and inserted into a BsaI-digested pGGC000 plasmid via ligation.

The unarmed gRNA modules were cloned by amplifying the AtU6-26 promoter and gRNA scaffold from previously described Golden Gate entry vectors (Houbaert et al., 2018). The amplification was performed using the forward primer 120 and the reverse primers 283, 284, 230, 231, 232, and 233 for the B to G overhangs, respectively. This removed an unwanted attB2 site. The PCR products were digested with BsaI and ligated into the respective empty entry vectors. The unarmed gRNA modules were further adapted by adding the *ccd*B negative selectable marker. The *ccd*B gene was PCR amplified from pEN-L1-AG-L2 with oligos 391 and 392 and

inserted into BbsI-digested unarmed gRNA modules via Gibson assembly. pGG-F-AtU6-26-AarI-AarI-G was produced by annealing oligos 345 and 346 and ligating these into the BbsI-digested vector pGG-F-AtU6-26-BbsI-Bbs-G.

The linker modules for Golden Gate were constructed as previously described (Houbaert et al., 2018). The entry module pGG-F-A-AarI-AarI-G-G was generated by annealing oligos 361 and 362 and ligating into the BsaI-digested entry vector pGGF000. The variable linker pGG-F-A-AarI-SacB-AarI-G-G, based on the SacB sequence from pMA7-SacB (Lennen et al., 2016), was synthesized on the BioXP3200 DNA synthesis platform (SGI-DNA) and inserted into a BsaI-digested pGGF000 plasmid via Gibson assembly.

The variable linker modules were constructed by PCR-amplifying the AarI-SacB fragment from pGG-F-A-AarI-SacB-AarI-G-G with the respective primers 1589 to 1600 (Supplemental Data Set 10). The PCR products were gel purified and inserted via Gibson assembly into a modified pDONR207 vector (Invitrogen) predigested with ApaI and SacI. Clones were verified with oligo 1658.

GATEWAY Destination Vectors

pGG-A-pOLE1-B, pGG-B-OLE1-C, pGG-D-linker-E (Lampropoulos et al., 2013), pGG-E-NOST-F, and pGG-F-LinkerII-G were assembled into pEN-L1-A-G-L2 with pGG-C-mRuby3-D or pGG-C-GFP-D (Lampropoulos et al., 2013). The ligation reactions were used as templates for PCR with the primers 195 and 196. The PCR products were cloned via Gibson assembly into pGGK7m24GW (Karimi et al., 2005) linearized with KpnI and XbaI. Clones were verified by Sanger sequencing. The resulting vectors containing the red and green fluorescent FAST markers were named pFASTRK24GW and pFASTGK24GW, respectively.

Proof-of-Concept Vectors

The Golden Gate entry modules pGG-A-*pSMB*-B, pGG-B-Linker-C, pGG-C-Cas9PTA*-D, pGG-D-Linker-E, pGG-E-G7T-F, and pGG-F-linkerII-G were assembled in pEN-L4-AG-R1 (Houbaert et al., 2018), resulting in the vector pEN-L4-*pSMB*-Cas9PTA-G7T-R1. The Golden Gate entry modules pGG-A-AtU6-26-BbsI-BbsI-B and pGG-B-linkerII-G were assembled in pEN-L1-A-G-L2 (Houbaert et al., 2018), resulting in the vector pEN-L1-AtU6-26-BbsI-BbsI-L2. The BbsI restriction sites were swapped with a fragment containing the *ccd*B and *Cm*R selectable markers flanked with BsaI sites. This fragment was PCR amplified from the plasmid pEN-L4-A-G-R1, using primers 1436 and 1437. The fragment was BsaI-digested and ligated with T4 DNA Ligase in the BbsI-digested vector pEN-L1-AtU6-26-BbsI-BbsI-L2, resulting in the vector pEN-L1-AtU6-26-BsaI-BsaI-L2. pEN-L4-*pSMB*-Cas9PTA-G7T-R1 and pEN-L1-AtU6-26-BsaI-BsaI-L2 were recombined in pGGB7m24GW (Karimi et al., 2005) via a MultiSite Gateway reaction according to manufacturer's recommendations. This vector was called pB-*pSMB*-Cas9-G7T-AtU6-BsaI-BsaI-gRNA scaffold.

Oligos 138 and 139 (GFP-1 target) and oligos 134 and 135 (GFP-2 target) were annealed by adding 1 μL of each 100 μM oligonucleotide in 48 μL of ultra-pure water and incubating with a slow cooling program on the thermal cycler (5 min at 95°C; 95 to 85°C, −2°C/s; 85 to 25°C, −0.1°C/s). These annealed oligonucleotides were cloned via a Golden Gate reaction into pB-*pSMB*-Cas9-G7T-AtU6-BsaI-BsaI-gRNA scaffold. The Golden Gate reaction conditions are described in the Supplemental Protocol. The resulting vectors were named pB-*pSMB*-Cas9-G7T-AtU6-GFP-1 and GFP-2.

Golden Gate Destination Vectors

The Golden Gate destination vectors were cloned by amplifying the *Cm*R and *ccd*B selection cassettes, flanked by the Golden Gate cloning sites A to G, from pEN-L1-AG-L2 using primers 298 and 313. The PCR products were

column purified and cloned via Gibson assembly in the HindIII and PstI linearized Gateway destination vectors pGGP7m24GW, pGGK7m24GW, pGGB7m24GW, pGGPH7m24GW (Karimi et al., 2005), pFASTRK24GW, and pFASTGK24GW. The resulting vectors were named pGGP A-G, pGGK A-G, pGGB A-G, pGGH A-G, pFASTRK A-G, and pFASTGK A-G, respectively. All clones were verified by Sanger sequencing and diagnostic digestion with NotI.

To generate the pFASTR-A-G destination vector, the Golden Gate entry modules pGG-A-pOLE1-B, pGG-B-OLE1-C, pGG-C-mRuby3-D, pGG-D-Linker-E, pGG-E-NOST-F, and pGG-F-linkerII-G were assembled in pGGP A-G. Subsequently, the *Cm*R and *ccd*B selection cassettes, flanked by the Golden Gate cloning sites, were PCR amplified using primers 298 and 430 from pEN-L1-AG-L2 and inserted via Gibson assembly.

One-Step CRISPR-TSKO Cloning Vectors

To clone the two gRNAs in a destination vector, we followed a similar approach as previously described (Xing et al., 2014), with some modifications. A plasmid was generated to serve as a PCR template for 2-gRNA vectors. The Golden Gate entry modules pGG-A-AtU6-26-BbsI-BbsI-B, pGG-B-Linker-C (Lampropoulos et al., 2013), pGG-B-AtU6PTA-C (Houbaert et al., 2018), and pGG-D-linkerII-G were assembled in pEN-L1-A-G-L2 to generate pEN-2xAtU6 template. The clone was verified by Sanger sequencing.

The extended protocol for one-step, CRISPR-TSKO cloning vectors can be found in the Supplemental Protocol. In summary, six different entry modules are combined via Golden Gate assembly in a destination vector. The A-B entry module contains the tissue-specific promotor, the C-D module contains the Cas9 endonuclease and can be combined with an N-terminal tag (B-C) or C-terminal tag (D-E), and the E-F entry module contains the terminator. To construct a vector that is compatible with cloning one or two gRNAs, the F-G module pGG-F-AtU6-26-AarI-AarI-G is used (Figure 1). Upon digestion with AarI, this vector can be loaded directly with one or two gRNAs. Alternatively, the AarI sites can be replaced with a fragment containing BsaI sites flanking the *ccd*B and *Cm*R selectable markers. Two gRNAs can be cloned via a PCR on the pEN-2xAtU6 template using primers that contain gRNA spacer sequences via a Golden Gate reaction. More details can be found in the Supplemental Protocol.

To construct a vector that is compatible with multiple gRNAs (up to 12), the Golden Gate cloning method is slightly modified. The initial Golden Gate reaction is performed with an F-G linker containing AarI restriction sites (Supplemental Figure 2). Upon AarI digestion, this vector can be directly loaded with six Golden Gate entry modules containing one or two AtU6-26 promotors and gRNAs. Alternatively, a similar strategy to replace the AarI sites by the *ccd*B and *Cm*R selectable markers flanked with BsaI sites can be followed. All gRNA target sequences are shown in the Supplemental Table.

Expression Vector with an Empty Promoter Module

The armed gRNA module pGG-F-AtU6-26-GFP-1-G was produced by annealing oligos 138 and 139 (GFP-1 target) and ligating these via a Golden Gate reaction in pGG-F-AtU6-26-BbsI-ccdB-BbsI-G. The entry modules pGG-A-AarI-SacB-AarI-B, pGG-B-Linker-C, pGG-C-Cas9PTA*-D, pGG-D-P2A-mCherry-NLS-E, pGG-E-G7T-F, and pGG-F-AtU6-26-GFP-1-G were cloned into pFASTR A-G via a Golden Gate reaction. This vector was digested with AarI, and the upper band was gel purified. The PCR product of the reaction with pEN-L4-AG-R1 using oligos 1879 and 1880 was cloned into the AarI-digested fragment using Gibson assembly. The resulting vector, pFASTR-BsaI-CmR-ccdB-BsaI-Cas9-P2A-mCherry-G7T-AtU6-GFP-1, was verified by restriction digest using PvuII and sequencing. Entry modules containing a promoter can easily be cloned in this vector via a Golden Gate reaction.

Plant Lines Used in This Study

The Arabidopsis (*Arabidopsis thaliana*) *smb-3* line was derived from the SALK collection (SALK_143526C). The NLS-GFP line (pHTR5:NLS-GFP-GUS) was previously reported (Ingouff et al., 2017) and was deposited in the NASC collection (N2109788). Note, the line was initially named pHTR5:NLS-GUS-GFP, but the GFP is on the N-terminal side of GUS and we are renaming it accordingly here. The *arf7 arf19* double mutant (Okushima et al., 2005) was derived from the ABRC collection (CS24629). The *yda-1* mutant was previously reported (Lukowitz et al., 2004).

Plant Transformation

Plant vectors were transformed in *Agrobacterium tumefaciens* C58C1 by electroporation. Transformation in pHTR5:NLS-GFP-GUS was performed via the floral-dip method (Clough and Bent, 1998). For constructs containing the bar selectable marker, T1 seeds were selected on half strength Murashige and Skoog (MS) medium + 10 mgL^{-1} Glufosinate-ammonium (Sigma-Aldrich). For the construct containing the FASTR screenable marker, T1 transgenic seeds were selected under a Leica M165FC fluorescence stereomicroscope. Resistant seedlings or FASTR-positive seeds were transferred to Jiffy-7 pellets and grown in a greenhouse at 21°C under a 16-h day regime (100 Wm^{-2} photosynthetically active radiation) from natural light complemented with 600-W GreenPower (Philips) high-pressure sodium lightbulbs. Seedlings used for phenotypic analyses were grown in vitro on half strength MS medium inside 21°C growth chambers under continuous light from SpectraluxPlus NL 36 W/ 840 Plus (Radium Lampenwerk) fluorescent bulbs.

DNA Extraction and Molecular Analysis

Seedling, leaves, or roots were frozen and ground into powder using a TissueLyser (Retsch MM300). DNA was extracted using a modified version of the protocol from Edwards et al. (1991). The modifications consisted of an adapted extraction buffer (100 mM Tris HCl, pH 8.0, 500 mM NaCl, 50 mM EDTA, 0.7% [w/v] SDS) and a 70% (v/v) ethanol washing step before dissolving the pellet. A region around the CRISPR/Cas9 target site was PCR amplified using ALLin Red Taq Master Mix, 2X (highQu) with the following program on the thermocycler: 95°C for 3 min, followed by 33 cycles (30 s at 95°C, 30 s at the annealing temperature, 1 min/kb at 72°C), 72°C for 5 min. The PCR products were analyzed via agarose gel electrophoresis, and the cleanup was done by bead purification with HighPrep PCR (MAGBIO) or column purification with a DNA Clean and Concentrator kit (Zymo Research). The purified samples were sent for Sanger sequencing (Eurofins Scientific) and analyzed using TIDE (version 2.0.1; Brinkman et al., 2014).

Confocal Microscopy for Original Proof of Concept

T1 seedlings were imaged on a LSM710 confocal microscope (Zeiss). GFP was excited at 488 nm and acquired at 500 to 550 nm. T2 seedlings were imaged on a Leica SP8X confocal microscope. GFP was excited at 488 nm and acquired at 500 to 530 nm.

Confocal Microscopy

Seedlings were imaged on a Leica SP8X confocal microscope. For root imaging, GFP was excited at 488 nm and acquired at 500 to 530 nm. mCherry was excited at 594 nm and acquired at 600 to 650 nm. Samples were stained with 20 µg/mL 4',6-diamidino-2-phenylindole (DAPI) or 10 µg/mL propidium iodide in 0.43 gL^{-1} MS salts with 94 µM MES.H$_2$O medium. DAPI was excited at 405 nm and acquired at 410 to 480 nm in sequential mode.

For stomata imaging, cotyledons were vacuum infiltrated with 20 μg/mL of DAPI in 0.43 gL^{-1} MS salts with 94 μM MES.H$_2$O medium. Samples were imaged in sequential mode. DAPI was excited at 405 nm and acquired at 410 to 450 nm. GFP was excited at 488 nm and acquired at 500 to 530 nm. mCherry was excited at 594 nm and acquired at 600 to 650 nm. Chlorophyll fluorescence was excited at 488 nm and acquired at 680 to 730 nm. Images were analyzed using Fiji (Schindelin et al., 2012).

To image lateral root primordia, seedlings were cleared using the ClearSee protocol (Kurihara et al., 2015; Ursache et al., 2018) in combination with cell wall staining using Calcofluor White M2R (Sigma) on a Leica SP8X confocal microscope. Calcofluor White was excited at 405 nm and acquired at 430 to 470 nm. GFP was excited at 488 nm and acquired at 500 to 525 nm. mCherry was excited at 594 nm and acquired at 600 to 630 nm.

Epifluorescence Microscopy

Cotyledons of FASTR-positive seedlings were mounted on distilled water and observed on a Zeiss Observer.Z1 using a Plan-Apochromat 20×/0.8 DICII objective. GFP fluorescence was observed with a band pass (BP) 470/40 filter for excitation, a FT 495 beam splitter, and a BP 525/50 emission filter. mCherry was observed with a BP 545/25 filter for excitation, a FT 570 beam splitter, and a BP 605/70 emission filter.

Segmentation and Analysis of Root Cap Nuclei

Root tip image stacks were segmented and nuclei intensity measurements performed using the interactive learning and segmentation toolkit ilastik 1.3.0 (Sommer et al., 2011). GFP and mCherry intensities were measured for segmented nuclei with a probability equal or greater than 0.95 of belonging to root cap cells. Based on mCherry measurements in the NLS-GFP line, a threshold of 25 was established as a minimum signal for mCherry.

Protoplast Preparation and Cell Sorting

Arabidopsis protoplasts were prepared as previously described (Bargmann and Birnbaum, 2010). In brief, for *pSMB*-CRISPR-TSKO lines, root tips of 600 5 DAG seedlings grown under continuous light on 0.43 gL^{-1} MS salts with 94 μM MES.H$_2$O medium were incubated in protoplasting solution consisting of 1.25% (w/v) cellulase (Yakult), 0.3% (w/v) Macerozyme (Yakult), 0.4 M mannitol, 20 mM MES, 20 mM KCl, 0.1% (w/v) BSA, and 10 mM CaCl$_2$ at pH 5.7 for 3 h. The samples were filtered through a 40-μm filter and the flow-through centrifuged at 150g for 10 min. The supernatant was discarded and protoplasts were recovered in ice-cold resuspension buffer. Resuspension buffer was of the same constitution as protoplasting buffer, with the omission of both cellulase and macerozyme. For lines targeting stomatal lineages, cotyledons of 600 5 DAG seedlings were processed as above but with a 12-h incubation time to ensure the proper release of guard cells.

Root tip protoplasts were sorted into 1.5-mL Eppendorf tubes containing 500 μL of resuspension buffer using a BD FACSArialI equipped with three lasers (405 nm, 488 nm, and 633 nm). To account for the double presence of GFP and mCherry in some samples, the cotyledon protoplasts were sorted into 1.5 mL Eppendorf tubes containing 500 μL of resuspension buffer using a BD FACSMelody equipped with three lasers (405 nm, 488 nm, and 561 nm). The 561-nm laser in the BD FACSMelody made better separation possible due to a better excitation of the mCherry. All FACS sorting reports can be found in Supplemental Figures 6 and 7.

Quantification of Lateral Root Density

Seeds were sown on half-strength MS medium (Duchefa Biochemie) supplemented with 1% (w/v) Suc and 0.8% (w/v) agar, pH 5.7, and stratified for 2 d in the dark at 4°C. Seedlings were grown vertically for 12 d in continuous light (100 μmol m^{-2}s^{-1}) at 22°C. Presence/absence of Cas9-mCherry signal was scored using a Leica M165FC fluorescence stereomicroscope. The number of emerged lateral roots was determined for every seedling using a stereo microscope, and root lengths were measured via Fiji (ImageJ 1.52n; Schindelin et al., 2012) using digital images obtained by scanning the Petri dishes.

Stomata Analysis of Cotyledons in *YDA* Targeting Lines

The cotyledon epidermis of seedlings 10 d postgermination was visualized by clearing cotyledons in 100% (v/v) ethanol and incubating them at 60°C in 90% (v/v) ethanol/10% (v/v) acetic acid for 30 min and ethanol/1.25 M sodium hydroxide (1:1 [v/v]) for 2 h. The cleared cotyledons were incubated overnight at room temperature in lactic acid saturated with chloral hydrate, washed in 100% (v/v) lactic acid, and mounted for differential interference contrast microscopy (Olympus BX51). Images (430 μm × 566 μm) from the midlines to the margins on abaxial surfaces were generated. Thirty-five to 40 cotyledons of individual seedlings were evaluated per genotype.

Statistical Analysis

For segmentation and analysis of root cap nuclei, Spearman's correlation coefficient between median root cap signal of GFP and mCherry was calculated using SAS (Version 9.4, SAS Institute, 2013). For the comparison of emerged lateral root densities, the number of emerged lateral roots was modeled by Poisson regression using the primary root length as an offset variable and genotype as a fixed effect. In the presence of overdispersion, the negative binomial distribution was used instead of the Poisson distribution. The analysis was performed with the genmod procedure from SAS (SAS/STAT analytical product 14.3, SAS Institute, 2017). Post-hoc comparison tests were done using the capabilities of the plm procedure. For multiple testing, P values were adjusted using the Dunnett's method. For the comparison of lateral root lengths, a random-effects model was used to estimate the effect within each line. The root length was log transformed to stabilize the variance. Numerator degrees of freedom for the type III test of effect were calculated according to Kenward-Rogers as implemented in the mixed procedure from SAS (Version 9.4, SAS Institute, 2013). The assumptions were checked by residual diagnostics. The SAS code is available upon request.

Accession Numbers

Gene models used in this article can be found in the Arabidopsis Genome Initiative database under the following accession numbers: SMB (AT1G79580); TMM (AT1G80080); FAMA (AT3G24140); PDS3 (AT4G14210); YDA (AT1G63700); GATA23 (AT5G26930); ARF7 (AT5G20730); ARF19 (AT1G19220); CDKA;1 (AT3G48750); CDKB1;1 (AT3G54180); CDKB1;2 (AT2G38620)

Seeds for the line *pHTR5:NLS-GFP-GUS* are available from the Nottingham Arabidopsis Stock Centre (NASC), ID N2109788.

Supplemental Data

Supplemental Figure 1. Root cap-specific knockout of *GFP*

Supplemental Figure 2. Overview of the cloning scheme for constructing a vector with multiple gRNAs

Supplemental Figure 3. *GFP* and *SMB* knockout in root caps in the T1 and T2 generations

Supplemental Figure 4. Gene knockout in the stomatal lineage

ACKNOWLEDGMENTS

AUTHOR CONTRIBUTIONS

W.D., R.A.B., M.K.N., and T.B.J. conceived and devised the study. M.K. adapted the GreenGate vectors and provided additional cloning support. W.D. constructed the vectors and performed the genotyping analysis. R.A.B., M.L.P., N.V., and J.J. performed the experiments, imaging, and analysis. W.D., J.J., and R.A.B. performed statistical analysis. G.V.I. and R.A.B. performed the FACS experiments and analysis. W.D., T.B.J., R.A.B., M.K.N., and T.B. wrote the article with contributions from all other authors.

REFERENCES

Ablain, J., Durand, E.M., Yang, S., Zhou, Y., and Zon, L.I. (2015). A CRISPR/Cas9 vector system for tissue-specific gene disruption in zebrafish. Dev. Cell **32:** 756–764.

Allen, F., et al. (2018) Predicting the mutations generated by repair of Cas9-induced double-strand breaks. Nat. Biotechnol. **37:** 64.

Alvarez, J.P., Pekker, I., Goldshmidt, A., Blum, E., Amsellem, Z., and Eshed, Y. (2006). Endogenous and synthetic microRNAs stimulate simultaneous, efficient, and localized regulation of multiple targets in diverse species. Plant Cell **18:** 1134–1151.

Bargmann, B.O.R., and Birnbaum, K.D. (2010). Fluorescence activated cell sorting of plant protoplasts. J. Vis. Exp. **18:** e1673.

Barton, K.A., Schattat, M.H., Jakob, T., Hause, G., Wilhelm, C., Mckenna, J.F., Máthé, C., Runions, J., Van Damme, D., and Mathur, J. (2016). Epidermal pavement cells of Arabidopsis have chloroplasts. Plant Physiol. **171:** 723–726.

Bennett, T., van den Toorn, A., Sanchez-Perez, G.F., Campilho, A., Willemsen, V., Snel, B., and Scheres, B. (2010). SOMBRERO, BEARSKIN1, and BEARSKIN2 regulate root cap maturation in Arabidopsis. Plant Cell **22:** 640–654.

Bergmann, D.C., Lukowitz, W., and Somerville, C.R. (2004). Stomatal development and pattern controlled by a MAPKK kinase. Science **304:** 1494–1497.

Bortesi, L., and Fischer, R. (2015). The CRISPR/Cas9 system for plant genome editing and beyond. Biotechnol. Adv. **33:** 41–52.

Brinkman, E.K., Chen, T., Amendola, M., and van Steensel, B. (2014). Easy quantitative assessment of genome editing by sequence trace decomposition. Nucleic Acids Res. **42:** e168.

Burgos-Rivera, B., and Dawe, R.K. (2012). An *Arabidopsis* tissue-specific RNAi method for studying genes essential to mitosis. PLoS One **7:** e51388.

Carroll, K.J., Makarewich, C.A., McAnally, J., Anderson, D.M., Zentilin, L., Liu, N., Giacca, M., Bassel-Duby, R., and Olson, E.N. (2016). A mouse model for adult cardiac-specific gene deletion with CRISPR/Cas9. Proc. Natl. Acad. Sci. USA **113:** 338–343.

Čermák, T., Curtin, S.J., Gil-Humanes, J., Čegan, R., Kono, T.J.Y., Konečná, E., Belanto, J.J., Starker, C.G., Mathre, J.W., Greenstein, R.L., and Voytas, D.F. (2017). A multipurpose toolkit to enable advanced genome engineering in plants. Plant Cell **29:** 1196–1217.

Clough, S.J., and Bent, A.F. (1998). Floral dip: A simplified method for *Agrobacterium*-mediated transformation of *Arabidopsis thaliana*. Plant J. **16:** 735–743.

De Rybel, B., et al. (2010) A novel aux/IAA28 signaling cascade activates GATA23-dependent specification of lateral root founder cell identity. Curr. Biol. **20:** 1697–1706.

De Smet, I., et al. (2010) Bimodular auxin response controls organogenesis in *Arabidopsis*. Proc. Natl. Acad. Sci. USA **107:** 2705–2710.

De Veylder, L., Beeckman, T., and Inzé, D. (2007). The ins and outs of the plant cell cycle. Nat. Rev. Mol. Cell Biol. **8:** 655–665.

Denyer, T., Ma, X., Klesen, S., Scacchi, E., Nieselt, K., and Timmermans, M.C.P. (2019). Spatiotemporal developmental trajectories in the *Arabidopsis* root revealed using high-throughput single-cell RNA sequencing. Dev. Cell **48:** 840–852.e5.

Edwards, K., Johnstone, C., and Thompson, C. (1991). A simple and rapid method for the preparation of plant genomic DNA for PCR analysis. Nucleic Acids Res. **19:** 1349.

Endo, M., Mikami, M., and Toki, S. (2015). Multigene knockout utilizing off-target mutations of the CRISPR/Cas9 system in rice. Plant Cell Physiol. **56:** 41–47.

Engler, C., Kandzia, R., and Marillonnet, S. (2008). A one pot, one step, precision cloning method with high throughput capability. PLoS One **3:** e3647.

Fendrych, M., Van Hautegem, T., Van Durme, M., Olvera-Carrillo, Y., Huysmans, M., Karimi, M., Lippens, S., Guérin, C.J., Krebs, M., Schumacher, K., and Nowack, M.K. (2014). Programmed cell death controlled by ANAC033/SOMBRERO determines root cap organ size in *Arabidopsis*. Curr. Biol. **24:** 931–940.

Fu, J.L., Kanno, T., Liang, S.C., Matzke, A.J.M., and Matzke, M. (2015). GFP loss-of-function mutations in *Arabidopsis thaliana*. G3 (Bethesda) **5:** 1849–1855.

Fukaki, H., Nakao, Y., Okushima, Y., Theologis, A., and Tasaka, M. (2005). Tissue-specific expression of stabilized SOLITARY-ROOT/IAA14 alters lateral root development in *Arabidopsis*. Plant J. **44:** 382–395.

Hauser, F., Chen, W., Deinlein, U., Chang, K., Ossowski, S., Fitz, J., Hannon, G.J., and Schroeder, J.I. (2013). A genomic-scale artificial microRNA library as a tool to investigate the functionally redundant gene space in Arabidopsis. Plant Cell **25:** 2848–2863.

Houbaert, A., et al. (2018) POLAR-guided signaling complex assembly and localization drive asymmetric cell division. Nature **563:** 574–578.

Hyun, Y., Kim, J., Cho, S.W., Choi, Y., Kim, J.S., and Coupland, G. (2015). Site-directed mutagenesis in *Arabidopsis thaliana* using dividing tissue-targeted RGEN of the CRISPR/Cas system to generate heritable null alleles. Planta **241:** 271–284.

Ingouf, M., Selles, B., Michaud, C., Vu, T.M., Berger, F., Schorn, A.J., Autran, D., Van Durme, M., Nowack, M.K., Martienssen, R.A., and Grimanelli, D. (2017). Live-cell analysis of DNA methylation during sexual reproduction in *Arabidopsis* reveals context and sex-specific dynamics controlled by noncanonical RdDM. Genes Dev. **31:** 72–83.

Inze, D., and De Veylder, L. (2006). Cell cycle regulation in plant development. Annu. Rev. Genet. **40:** 77–105.

Jinek, M., Chylinski, K., Fonfara, I., Hauer, M., Doudna, J.A., and Charpentier, E. (2012). A programmable dual-RNA-guided DNA endonuclease in adaptive bacterial immunity. Science **337:** 816–821.

Karimi, M., De Meyer, B., and Hilson, P. (2005). Modular cloning in plant cells. Trends Plant Sci. **10:** 103–105.

Kerschen, A., Napoli, C.A., Jorgensen, R.A., and Müller, A.E. (2004). Effectiveness of RNA interference in transgenic plants. FEBS Lett. **566:** 223–228.

Kumpf, R.P., and Nowack, M.K. (2015). The root cap: A short story of life and death. J. Exp. Bot. **66:** 5651–5662.

Kurihara, D., Mizuta, Y., Sato, Y., and Higashiyama, T. (2015). ClearSee: A rapid optical clearing reagent for whole-plant fluorescence imaging. Development **142:** 4168–4179.

Kushwaha, N.K., and Chakraborty, S. (2017). Chilli leaf curl virus-based vector for phloem-specific silencing of endogenous genes and overexpression of foreign genes. Appl. Microbiol. Biotechnol. **101:** 2121–2129.

Lampropoulos, A., Sutikovic, Z., Wenzl, C., Maegele, I., Lohmann, J.U., and Forner, J. (2013). GreenGate—a novel, versatile, and efficient cloning system for plant transgenesis. PLoS One **8:** e83043.

Lavenus, J., Goh, T., Roberts, I., Guyomarc'h, S., Lucas, M., De Smet, I., Fukaki, H., Beeckman, T., Bennett, M., and Laplaze, L. (2013). Lateral root development in Arabidopsis: Fifty shades of auxin. Trends Plant Sci. **18:** 450–458.

Lawson, T. (2009). Guard cell photosynthesis and stomatal function. New Phytol. **181:** 13–34.

Lennen, R.M., Nilsson Wallin, A.I., Pedersen, M., Bonde, M., Luo, H., Herrgård, M.J., and Sommer, M.O.A. (2016). Transient over-expression of DNA adenine methylase enables efficient and mobile genome engineering with reduced off-target effects. Nucleic Acids Res. **44:** e36.

Liang, Y., Eudes, A., Yogiswara, S., Jing, B., Benites, V.T., Yamanaka, R., Cheng-Yue, C., Baidoo, E.E., Mortimer, J.C., Scheller, H.V., and Loqué, D. (2019). A screening method to identify efficient sgRNAs in *Arabidopsis*, used in conjunction with cell-specific lignin reduction. Biotechnol. Biofuels **12:** 130.

Lloyd, J.P., Seddon, A.E., Moghe, G.D., Simenc, M.C., and Shiu, S.H. (2015). Characteristics of plant essential genes allow for within- and between-species prediction of lethal mutant phenotypes. Plant Cell **27:** 2133–2147.

Lowder, L.G., Zhang, D., Baltes, N.J., Paul, J.W., III, Tang, X., Zheng, X., Voytas, D.F., Hsieh, T.F., Zhang, Y., and Qi, Y. (2015). A CRISPR/Cas9 toolbox for multiplexed plant genome editing and transcriptional regulation. Plant Physiol. **169:** 971–985.

Lukowitz, W., Roeder, A., Parmenter, D., and Somerville, C. (2004). A MAPKK kinase gene regulates extra-embryonic cell fate in *Arabidopsis*. Cell **116:** 109–119.

Mao, Y., Zhang, Z., Feng, Z., Wei, P., Zhang, H., Botella, J.R., and Zhu, J.K. (2016). Development of germ-line-specific CRISPR-Cas9 systems to improve the production of heritable gene modifications in *Arabidopsis*. Plant Biotechnol. J. **14:** 519–532.

Marzec, M., and Hensel, G. (2018). Targeted base editing systems are available for plants. Trends Plant Sci. **23:** 955–957.

Melnyk, C.W., Molnar, A., and Baulcombe, D.C. (2011). Intercellular and systemic movement of RNA silencing signals. EMBO J. **30:** 3553–3563.

Mitsuda, N., Matsui, K., Ikeda, M., Nakata, M., Oshima, Y., Nagatoshi, Y., and Ohme-Takagi, M. (2011). CRES-T, an effective gene silencing system utilizing chimeric repressors. In Plant Transcription Factors: Methods and Protocols, L. Yuan, and and S.E. Perry, eds (Totowa, NJ: Humana Press), pp. 87–105.

Muñoz-Nortes, T., Candela, H., and Micol, J.L. (2017). Suitability of two distinct approaches for the high-throughput study of the post-embryonic effects of embryo-lethal mutations in *Arabidopsis*. Sci. Rep. **7:** 17010.

Musielak, T.J., and Bayer, M. (2014). YODA signalling in the early *Arabidopsis* embryo. Biochem. Soc. Trans. **42:** 408–412.

Nadeau, J.A., and Sack, F.D. (2002). Control of stomatal distribution on the *Arabidopsis* leaf surface. Science **296:** 1697–1700.

Negi, J., Munemasa, S., Song, B., Tadakuma, R., Fujita, M., Azoulay-Shemer, T., Engineer, C.B., Kusumi, K., Nishida, I., Schroeder, J.I., and Iba, K. (2018). Eukaryotic lipid metabolic pathway is essential for functional chloroplasts and CO_2 and light responses in *Arabidopsis* guard cells. Proc. Natl. Acad. Sci. USA **115:** 9038–9043.

Nowack, M.K., Harashima, H., Dissmeyer, N., Zhao, X., Bouyer, D., Weimer, A.K., De Winter, F., Yang, F., and Schnittger, A. (2012). Genetic framework of cyclin-dependent kinase function in *Arabidopsis*. Dev. Cell **22:** 1030–1040.

Ohashi-Ito, K., and Bergmann, D.C. (2006). Arabidopsis FAMA controls the final proliferation/differentiation switch during stomatal development. Plant Cell **18:** 2493–2505.

Okushima, Y., Fukaki, H., Onoda, M., Theologis, A., and Tasaka, M. (2007). ARF7 and ARF19 regulate lateral root formation via direct activation of LBD/ASL genes in Arabidopsis. Plant Cell **19:** 118–130.

Okushima, Y., et al. (2005) Functional genomic analysis of the AUXIN RESPONSE FACTOR gene family members in Arabidopsis thaliana: unique and overlapping functions of ARF7 and ARF19. Plant Cell **17:** 444–463.

Pasin, F., Kulasekaran, S., Natale, P., Simón-Mateo, C., and García, J.A. (2014). Rapid fluorescent reporter quantification by leaf disc analysis and its application in plant-virus studies. Plant Methods **10:** 22.

Port, F., Chen, H.M., Lee, T., and Bullock, S.L. (2014). Optimized CRISPR/Cas tools for efficient germline and somatic genome engineering in *Drosophila*. Proc. Natl. Acad. Sci. USA **111:** E2967–E2976.

Qin, G., Gu, H., Ma, L., Peng, Y., Deng, X.W., Chen, Z., and Qu, L.J. (2007). Disruption of phytoene desaturase gene results in albino and dwarf phenotypes in *Arabidopsis* by impairing chlorophyll, carotenoid, and gibberellin biosynthesis. Cell Res. **17:** 471–482.

Rademacher, E.H., Möller, B., Lokerse, A.S., Llavata-Peris, C.I., van den Berg, W., and Weijers, D. (2011). A cellular expression map of the Arabidopsis AUXIN RESPONSE FACTOR gene family. Plant J. **68:** 597–606.

Schindelin, J., et al. (2012) Fiji: An open-source platform for biological-image analysis. Nat. Methods **9:** 676–682.

Schürholz, A.K., et al. (2018) A comprehensive toolkit for inducible, cell type-specific gene expression in Arabidopsis. Plant Physiol. **178:** 40–53.

Schwab, R., Ossowski, S., Riester, M., Warthmann, N., and Weigel, D. (2006). Highly specific gene silencing by artificial microRNAs in Arabidopsis. Plant Cell **18:** 1121–1133.

Senthil-Kumar, M., and Mysore, K.S. (2011). New dimensions for VIGS in plant functional genomics. Trends Plant Sci. **16:** 656–665.

Shimada, T.L., Shimada, T., and Hara-Nishimura, I. (2010). A rapid and non-destructive screenable marker, FAST, for identifying transformed seeds of *Arabidopsis thaliana*. Plant J. **61:** 519–528.

Sieburth, L.E., Drews, G.N., and Meyerowitz, E.M. (1998). Non-autonomy of AGAMOUS function in flower development: Use of a Cre/loxP method for mosaic analysis in *Arabidopsis*. Development **125:** 4303–4312.

Smékalová, V., et al. (2014) Involvement of YODA and mitogen activated protein kinase 6 in *Arabidopsis* post-embryogenic root development through auxin up-regulation and cell division plane orientation. New Phytol. **203:** 1175–1193.

Smith, I., Greenside, P.G., Natoli, T., Lahr, D.L., Wadden, D., Tirosh, I., Narayan, R., Root, D.E., Golub, T.R., Subramanian, A., and Doench, J.G. (2017). Evaluation of RNAi and CRISPR technologies by large-scale gene expression profiling in the Connectivity Map. PLoS Biol. **15:** e2003213.

Sommer, C., Sträehle, C., Köthe, U., Hamprecht, F.A. (2011). Ilastik: Interactive learning and segmentation toolkit. In Eighth IEEE International Symposium on Biomedical Imaging (ISBI) Proceedings, pp. 230–233.

Ursache, R., Andersen, T.G., Marhavý, P., and Geldner, N. (2018). A protocol for combining fluorescent proteins with histological stains for diverse cell wall components. Plant J. **93:** 399–412.

von Wangenheim, D., Fangerau, J., Schmitz, A., Smith, R.S., Leitte, H., Stelzer, E.H.K., and Maizel, A. (2016). Rules and self-organizing properties of post-embryonic plant organ cell division patterns. Curr. Biol. **26:** 439–449.

Willemsen, V., Bauch, M., Bennett, T., Campilho, A., Wolkenfelt, H., Xu, J., Haseloff, J., and Scheres, B. (2008). The NAC domain transcription factors FEZ and SOMBRERO control the orientation of cell division plane in *Arabidopsis* root stem cells. Dev. Cell **15:** 913–922.

Xing, H.L., Dong, L., Wang, Z.P., Zhang, H.Y., Han, C.Y., Liu, B., Wang, X.C., and Chen, Q.J. (2014). A CRISPR/Cas9 toolkit for multiplex genome editing in plants. BMC Plant Biol. **14:** 327.

Yan, L., Wei, S., Wu, Y., Hu, R., Li, H., Yang, W., and Xie, Q. (2015). High-efficiency genome editing in *Arabidopsis* using YAO promoter-driven CRISPR/Cas9 system. Mol. Plant **8:** 1820–1823.

This information is current as of December 10, 2019

Supplemental Data	**/content/suppl/2019/09/28/tpc.19.00454.DC2.html** **/content/suppl/2019/09/27/tpc.19.00454.DC1.html**
References	This article cites 70 articles, 24 of which can be accessed free at: /content/31/12/2868.full.html#ref-list-1
Permissions	https://www.copyright.com/ccc/openurl.do?sid=pd_hw1532298X&issn=1532298X&WT.mc_id=pd_hw1532298X
eTOCs	Sign up for eTOCs at: http://www.plantcell.org/cgi/alerts/ctmain
CiteTrack Alerts	Sign up for CiteTrack Alerts at: http://www.plantcell.org/cgi/alerts/ctmain
Subscription Information	Subscription Information for *The Plant Cell* and *Plant Physiology* is available at: http://www.aspb.org/publications/subscriptions.cfm